SYNTHESES, SPECTROELECTROCHEMICAL AND ELECTROCHEMICAL CHARACTERIZATIONS OF NAPHTHODITHIOPHENE CONTAINING POLYMERS FOR SOLAR CELL APPLICATIONS

A THESIS SUBMITTED TO
THE GRADUATE SCHOOL OF NATURAL AND APPLIED SCIENCES
OF
MIDDLE EAST TECHNICAL UNIVERSITY

BY

EBRU IŞIK

IN PARTIAL FULFILLMENT OF THE REQUIREMENTS
FOR
THE DEGREE OF MASTER OF SCIENCE
IN
CHEMISTRY

AUGUST 2016

Approval of the thesis:

SYNTHESES, SPECTROELECTROCHEMICAL AND ELECTROCHEMICAL CHARACTERIZATIONS OF NAPHTHODITHIOPHENE CONTAINING POLYMERS FOR SOLAR CELL APPLICATIONS

submitted by **EBRU IŞIK** in partial fulfillment of the requirements for the degree of **Master of Science in Chemistry Department, Middle East Technical University** by,

Prof. Dr. Gülbin Dural Ünver _____
Dean, Graduate School of **Natural and Applied Sciences**

Prof. Dr. Cihangir Tanyeli _____
Head of Department, **Chemistry**

Prof. Dr. Levent Toppare _____
Supervisor, **Chemistry Dept., METU**

Examining Committee Members:

Assoc. Prof. Dr. Ali Çırpan _____
Chemistry Dept., METU

Prof. Dr. Levent Toppare _____
Chemistry Dept., METU

Assoc. Prof. Dr. Yasemin Arslan Udum _____
Advanced Technologies Dept., Gazi University

Assoc. Prof. Dr. İrem Erel Göktepe _____
Chemistry Dept., METU

Assist. Prof. Dr. Görkem Günbaş _____
Chemistry Dept., METU

Date: 26.08.2016

I hereby declare that all information in this document has been obtained and presented in accordance with academic rules and ethical conduct. I also declare that, as required by these rules and conduct, I have fully cited and referenced all material and results that are not original to this work.

Name, Last Name: Ebru IŞIK

Signature:

ABSTRACT

SYNTHESES, SPECTROELECTROCHEMICAL AND ELECTROCHEMICAL CHARACTERIZATIONS OF NAPHTHODITHIOPHENE CONTAINING POLYMERS FOR SOLAR CELL APPLICATIONS

Işık, Ebru

M. S., Department of Chemistry

Supervisor: Prof. Dr. Levent Toppare

August 2016, 87 pages

Naphthodithiophene is a thiophene fused naphthalene with a rigid and planar structure with extended π-conjugation system. Due its electron rich nature it has been recently employed in donor-acceptor type conducting polymers which are used as active layers in organic solar cells and organic field effect transistors. In this study alkoxy functionalized naphthodithiophene bearing two new random copolymers were designed and synthesized. As acceptor moiety in the polymer backbone electron deficient benzotriazole moiety was used. Thiophene and bithiophene units were used as π-linkers to enhance electron delocalization through polymer chain. Polymers were synthesized via Stille polycondensation reaction. Investigation of optoelectronic properties of synthesized polymers were performed with cyclic voltammetry and spectroelectrochemistry studies. Moreover, colorimetric and kinetic properties of the polymers were examined. From thiophene bridge to bithiophene bridge improvements in the properties of polymers were observed. Synthesized polymers were used as donor in bulk heterojunction organic solar cell applications together with $PC_{71}BM$ acceptor.

Polymer bearing bithiophene as π-bridge demonstrated 1.17% maximum power conversion efficiency.

Keywords: Naphthodithiophene, benzotriazole, π-bridge, random copolymer, organic solar cell

ÖZ

NAFTODİTİYOFEN İÇEREN POLİMERLERİN GÜNEŞ GÖZESİ UYGULAMARI İÇİN SENTEZİ, ELEKTROKİMYASAL VE SPEKTROELEKTROKİMYASAL KARAKTERİZASYONU

Işık, Ebru

Yüksek Lisans, Kimya Bölümü

Tez Yöneticisi: Prof. Dr. Levent Toppare

Ağustos 2016, 87 sayfa

Naftoditiyofen, planar ve sert yapıya ve genişletilmiş konjügasyona sahip tiyofen kaynaştırılmış naftalin grubundadır. Son zamanlarda naftoditiyofen ünitesi elektronca zengin yapısından dolayı organik alan etkili transistörler ve fotovoltaik uygulamalarda aktif alan olarak kullanılan donör-akseptör tipi konjüge polimerlerin sentezinde kullanılmaya başlamıştır. Bu çalışmada alkoksi grup fonksiyonlandırılmış naftoditiyofen içeren yeni rastgele kopolimerler sentezlenmiştir. Polimer omurgasında elektronca zayıf benzotriazol ünitesi elektron akseptör olarak kullanılmıştır. Polimer zincirinde elektron delokalizasyonunu arttırmak için tiyofen ve bitiyofen köprü üniteleri kullanılmıştır. Polimerler Stille kenetlenlenme reaksiyonu kullanılarak sentezlenmiştir. Sentezlenen polimerlerin optoelektronik özellikleri dönüşümlü voltametri ve spektroelektrokimya çalışmalarıyla incelenmiştir. Bunlara ek olarak, polimerlerin kolorimetrik ve kinetik özellikleri de incelenmiştir. Tiyofen köprü ünitesinden bitiyofen köprü ünitesine geçişte polimer özelliklerinde iyileşme gözlenmiştir. Sentezlenen polimerler organik güneş gözesi uygulamalarında aktif alan olarak kullanılmıştır. Bitiyofen köprü ünitesi içeren polimer maksimum % 1.17 güç çevirim verimi göstermiştir.

Anahtar Kelimeler: Naftoditiyofen, benzotriazol, köprü ünitesi, rastgele kopolimer, organik güneş gözesi

to my dear family

ACKNOWLEDGMENTS

I would like to thank my supervisor Prof. Dr. Levent Toppare for his guidance, support and encouragement throughout my studies. His discussions and advices will always worth. I am sincerely grateful to him for giving me the chance to work with him.

I would like to thank Assist. Prof. Dr. Görkem Günbaş for his valuable advices in organic synthesis whenever I needed.

I would like to thank Şerife Özdemir Hacıoğlu for her help in electrochemistry studies and answering all of my questions patiently.

I would like to thank Gönül Hızalan Özsoy for her contribution in organic solar cell studies as well as her valuable discussions.

I would like to express my special thanks to Seza Göker for teaching me organic synthesis, wonderful work environment and most importantly for her greatest friendship. She was always with me both as a mentor and as a friend every time I needed. Late night works, theatre activities and shopping are just few examples for our classics. I know that her endless support and friendship will be always with me and I will always be there for her wherever we are.

I would like to thank Merve İleri for being my best friend since undergraduate years, her indescribable support and friendship. We saved many happy memories together but they say you know your friends in the darkest times and she was always by my side in those times. Even though we are apart from each other I know that our friendship will never last.

I would like to thank Çağla İstanbulluoğlu my amazing lab mate, my lovely friend and my shoulder to cry on. I cannot describe the meaning of her infinite support and friendship all these years. Living the same ‘fate’ in every way made everything harder but our friendship was always there to make me smile and make me happy. I know that this friendship will continue from the other end of the world.

I would like to thank Melis Kesik Mancar for her continuous support and always listening me with a care. Coffee breaks, late night works with ‘Friends’ and sharing fun memories made these years much more enjoyable.

I would like to thank Janset Turan and Emre Ataoğlu for their incredible friendship, support and happy times. I hope that everything would be best for them and our friendship continues for long times.

I would like to thank Nehir Utku and Esra Özdemir for their friendship and happy memories through these years.

I would like to thank Seda Çömez and Saniye Söylemez for their kind friendship and coffee breaks.

I would like to thank Batuhan Balcı for being in my life, for his endless love and patience for me. I wish that we come together at the closest time and begin to our journey.

I cannot describe my gratitude to my parents, Saadet and Kemal Işık for their unconditional love and sacrifice through my life. Without their support nothing was possible. My special thanks go to my sisters, Elif and Esra Işık whom I am incredibly lucky to be in my life and always will be. Their endless support is meaningful than anything in this world.

TABLE OF CONTENTS

LIST OF TABLES

TABLES

LIST OF FIGURES

FIGURES

LIST OF ABBREVATIONS

ACN	Acetonitrile
AM 1.5 G	Air mass 1.5 Global
BTz	Benzotriazole
Bu_4NPF_6	Tetrabutylammonium hexafluorophosphate
$CDCl_3$	Deuterated chloroform
$CHCl_3$	Chloroform
CIE	International Commission on Illumination
CV	Cyclic Voltammetry
DCM	Dichloromethane
DIO	1,8-Diiodooctane
DMF	Dimethylformamide
E_g^{op}	Optical Band Gap
E_g^{el}	Electronic Band Gap
FF	Fill Factor
GPC	Gel Permeation Chromatography
HOMO	Highest Occupied Molecular Orbital
ITO	Indium Tin Oxide
IPCE	Incident Photon Current Efficiency
J_{sc}	Short Circuit Current
LUMO	Lowest Occupied Molecular Orbital
$MeNO_2$	Nitromethane

NDT	Naphthodithiophene
NHE	Normal Hydrogen Electrode
NMR	Nuclear Magnetic Resonance Spectroscopy
NIR	Near Infrared
OFET	Organic Field Effect Transistor
OLED	Organic Light Emitting Diode
PB	Prussian Blue
PCE	Power Conversion Efficiency
$\mathbf{P_{out}}$	Output Power
$\mathbf{P_{in}}$	Input Power
PEDOT	Polyethylene Dioxythiophene
PSS	Polystyrenesulfonate
$\mathbf{PC_{71}BM}$	[6,6]- Phenyl C71 butyric acid methyl ester
UV	Ultraviolet
Vis	Visible
$\mathbf{V_{oc}}$	Open Circuit Voltage
Z-NDT	Zigzag Naphthodithiophene

CHAPTER 1

INTRODUCTION

1.1. Conjugated Polymers

Π- Conjugated polymers are organic electro-active polymers, possessing single and double bonds alternatingly in their backbone. Overlap of p orbitals along the polymer chain creates electron delocalization through the polymer backbone, allowing the polymer to be electrically conductive in its doped states [1,2]. Advantages of these organic materials over their inorganic counterparts such as improved electronic properties, low cost, being solution processable, mechanical flexibility and tunable optical and electronic properties via structural modifications make them more demanding in recent years [2,3]. Discovery and development of conducting polymers brought Nobel Prize in Chemistry to Alan McDiarmid, Alan Heeger and Hideki Shirakawa in 2000. They have been able to prove that upon doping with iodine vapor the conductivity of polyacetylene resulted in a considerable increase in the order of 10^7[4,5]. Since polyacetylene was deprived of stability, heteroaromatic unit bearing more stable conjugated polymers have been developed over the years (Figure 1.1).

At their neutral (undoped) state, conjugated polymers are insulators, therefore polymers are needed to be doped either chemically or electrochemically to be conductive materials. During doping process dopant charges are introduced to polymer chain and they provide stabilization of the doped state. Electrons can be injected (n-doping) to polymer chain or can be removed (p-doping) from polymer backbone in order to achieve redox doping. Electrical and optical properties of conducting polymers can be modified with various doping levels and due to the

reversible nature of the process polymer backbone is not damaged throughout doping [6,7].

Conducting polymers have broad range of application areas which include organic solar cells, organic light emitting diodes (OLEDs), organic field effect transistors (OFETs), electrochromic devices and biosensors [8].

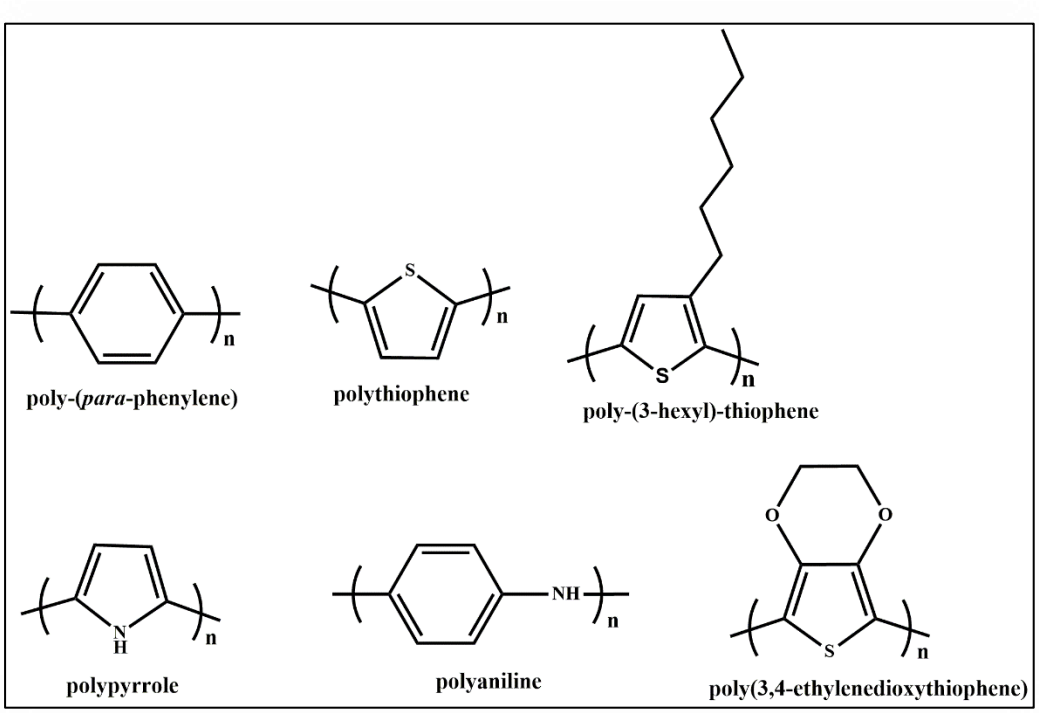

Figure 1.1. Structures of commonly employed conjugated polymers

1.2. Low Band Gap Polymers

Main application fields of π- conjugated conducting polymers such as organic photovoltaics [9], organic field effect transistors [10] and organic- light emitting diodes [11] are strictly influenced from the electronic and optical properties of polymers. Band gap which is the energy difference between the highest occupied molecular (HOMO) and lowest occupied molecular orbital (LUMO) is the key feature for conducting polymers to define their optoelectronic properties. According

to their conductivity level conjugated polymers are considered as semiconductors [12,13]. Orbital overlap and consequently electron delocalization through the polymer backbone becomes more facile as the band gap of polymer is lowered [14]. Therefore, it is essential to tune the band gap of polymers in a way to obtain desired optical and electronic properties to fulfill the requirements of application area in concern. Structural modifications in the main polymer chain enables to alter band gap of the conducting polymers [15]. One of the most commonly used method for this purpose is donor-acceptor approach in which polymers are constructed with the combination of electron-rich donor unit and electron-deficient acceptor unit in the same polymer backbone alternatingly [16,17]. In this strategy, while HOMO energy level of polymer is elevated by electron donor group, LUMO energy level is suppressed by electron deficient acceptor group causing reduced band gap demonstrated in Figure 1.2 [18].

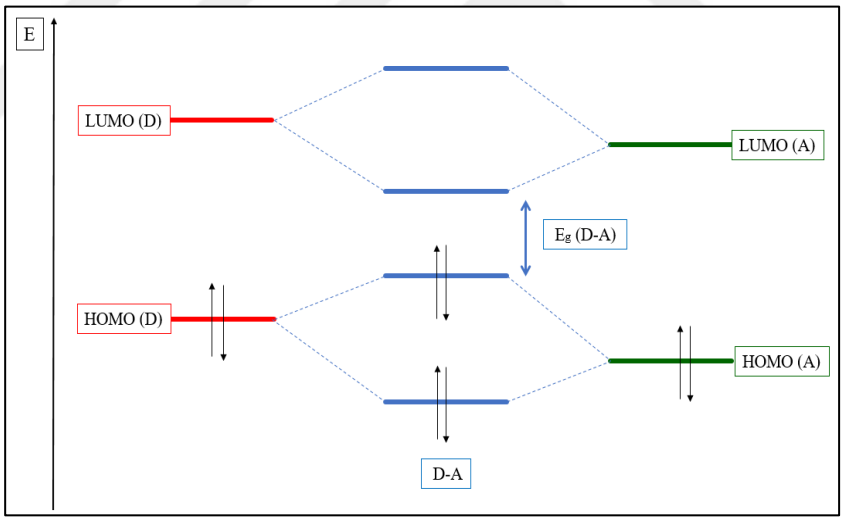

Figure 1.2. Orbital hybridization in donor-acceptor approach

1.3. Electrochromism and Electrochromic Materials

Electrochromism is a phenomenon in which different optical absorption bands are formed when the material experiences oxidation reduction reactions. Therefore,

materials that can undergo reversible color change with redox process are referred as electrochromic materials and they are commonly employed in electrochromic devices, displays and smart windows [19,20]. Electrochemically generated color change in the electrochromic materials occurs in a reversible and visible manner. Materials can be addressed as polyelectrochromic if more than two redox states are observed during redox reactions. Such materials demonstrate several newly formed colors at their different redox states [21]. There are various types of electrochromic materials existing such as transition metal oxides, viologens, Prussian blue and conjugated polymers [20].

Transition metal oxides are inorganic class of materials in which oxides of transition metals such as iridium, tungsten, rhodium, cobalt *etc.* show electrochromic behavior. Among them tungsten trioxide, WO_3, is the mostly studied one after its first report as an electrochromic material in 1969 [19,22]. WO_3 exhibits electrochromic property upon electrochemical reduction reaction. In its oxidized state WO_3 shows transparency however, when reduced electrochemically transparent thin film of WO_3 changes its color to blue. Electrochemical reaction for the general process is given below.

$$WO_3 + xM^+ + xe^- \longrightarrow MxWO_3$$

(transparent) (blue)

Even though WO_3 demonstrates color change with reduction, metal oxides of group VIII shows electrochromic behavior with electrochemical oxidation such as hydrated iridium oxide, $Ir(OH)_3$ [23].

1,1'-Disubstituted 4,4'-bipyridinium compounds commonly referred as viologens are another type of electrochromic materials possessing three different redox states with a color change(Figure 1.3) [24]. The most stable redox state of the viologens is colorless dication. When reversibly reduced to its radical cation form, radical is delocalized through the viologen system and the intramolecular charge transfer provides color change accompanied with a high intensity and high molar absorption coefficient. Substitutions in viologens are important in terms of the color of radical

cation. For instance, alkyl substitution on nitrogen creates blue/violet color whereas aryl groups offer green color to the radical dication [25].

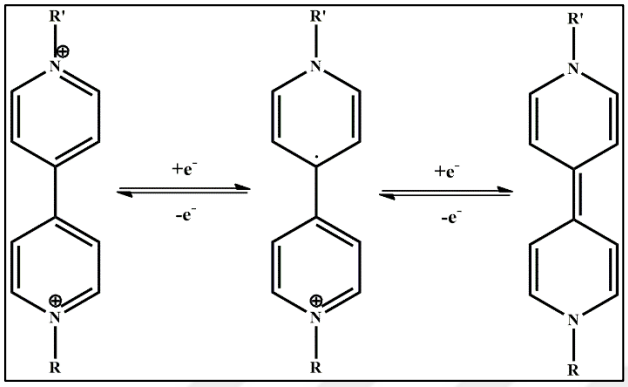

Figure 1.3. Redox states of viologens

Prussian blue (PB) iron(III) hexacyanoferrate(II), is an inorganic complex type of electrochromic material. Charge or electron transfer is possible in this system due to different oxidation numbers of the element, which is iron in PB. When the solution of iron(III) and hexacyanoferrate(III) is reduced electrochemically brown-yellow solution forms Prussian blue thin films with a reaction showed below [19,23].

$[Fe^{III}\,Fe^{III}(CN)_6] + e^- \longrightarrow [Fe^{III}\,Fe^{II}(CN)_6]^-$

Brown-yellow Blue

(Prussian brown) (Prussian blue)

As electrochromic materials conjugated polymers are more beneficial over inorganic ones in terms of providing high contrast ratios, fast response times, long life and high coloration efficiency [20]. Doping process with redox reaction in conjugated polymers creates color change between their undoped and doped states so that electrochromic behavior of conjugated polymers is observed. Since the optical properties of conjugated polymers are strongly influenced from the band gap of the material it is possible to tune the color change of polymers via structural modifications in the polymer backbone with use of synthetic organic chemistry. Ease

in tuning the band gap and consequently color of conjugated polymers is also an important advantage when compared with inorganic electrochromics [26,27].

1.4. Synthesis of Π-Conjugated Polymers

Conjugated polymers can be synthesized via electrochemical or chemical methods. Most popular methods in chemical synthesis are palladium catalyzed cross coupling reactions namely; Suzuki-Miyaura, Heck, Stille and Sonogashira reactions. Among them Suzuki and Stille cross coupling reactions are mostly preferred to obtain donor-acceptor type polymers [28].

1.4.1. Stille Polycondensation Reaction

Stille polycondensation reaction is an extensively used synthetic method for the preparation of conjugated polymers. The monomers involved in Stille cross coupling reaction have bifunctional units as organostannanes and organohalides. Stille reaction proceeds with a catalytic cycle of three step mechanism namely; oxidative addition, transmetallation and reductive elimination utilizing Pd (0) as the active catalyst. When Pd (II) is used as the catalyst, reaction starts with the activation of catalyst through reduction to Pd (0) by organostannyl groups and herewith a biaryl compound is formed. At the first step of Pd (0) mediated catalytic cycle, oxidative addition of organohalide unit to the active palladium catalyst takes place and Pd (II) intermediate is generated. The reaction process is followed by transmetallation step in which ligand substitution occurs on Pd (II) intermediate by cleavage of Sn-C bond. Transmetallation is considered as the rate-determining step for the Stille reaction. As a final step reductive elimination occurs to form product and the catalyst is regenerated to be utilized further in the reaction cycle. The total mechanism is demonstrated in Figure 1.4 [29].

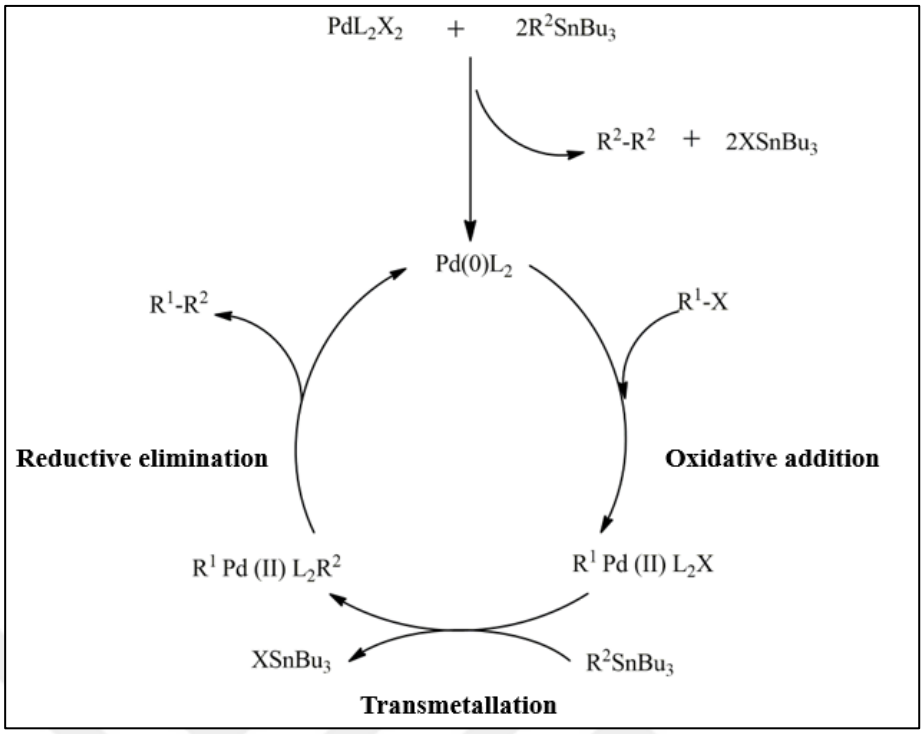

Figure 1.4. Mechanism of Stille polycondensation

Catalyst and reaction solvent are two important parameters affecting the Stille reaction. Despite its drawbacks, $Pd(PPh_3)_4$ is commonly preferred as catalyst in the Stille reaction. The catalyst lacks air stability so that the ligand, PPh_3, is easily oxidized to Ph_3PO even with very little amount of oxygen in the reaction medium. In addition, excess PPh_3 have inhibitor effect on the Stille reaction. $PdCl_2(PPh_3)_2$ can be employed as an alternative catalyst where the effect of PPh_3 is decreased, however it is much less air stable. $[Pd_2(dba)_3]$ is known to be more air stable and has been used in the Stille reaction in recent years [30]. Reaction solvent is significant because the polymer formed must be sustained in the medium as the reaction proceeds to obtain a high molecular weight. Also, catalyst stabilization is established by reaction solvent. Different types of solvents or solvent mixtures are utilized in Stille reaction and THF is one of the widely used solvent offering good solubility for both starting materials and resulting polymer and stabilization for the catalyst [31].

The reason for the wide employment of Stille reaction over other Pd mediated cross coupling reactions is its prominent advantages. Stille reaction requires mild reaction conditions and it is tolerable to different functional groups so that polymers containing different functional groups can be synthesized. Facility in the preparation of organohalides and organostannanes and more oxygen-moisture stable nature of organostannanes over other organometallics make Stille reaction more advantageous. Though the Stille reaction has featured advantages, it has some drawbacks as well. Organotin compounds are sensitive to silica gel therefore purification of them via column chromatography may create a problem. Also organotin compounds are highly toxic materials for health an environment [32].

1.4.2. Suzuki Polycondensation Reaction

Suzuki polycondensation reaction involves a cross coupling reaction of organohalides with organoboron compounds which are boronic acids or esters. It has a wide utilization area for carbon-carbon bond forming process. Similar to the Stille reaction, in Suzuki polycondensation Pd (0) is also used as the catalyst and catalytic reaction cycle involves the oxidative addition, transmetalation and reductive elimination steps. In Suzuki reaction base is employed in the reaction mechanism and it also involves in the catalytic cycle. Base is believed to generate reactive boronate compounds that interact with catalyst center in transmetalation step so that transmetalation occurs in an intramolecular way (Path A). Another proposal for the use of base is that it is replaced with a halide on the Pd (II) intermediate for intramolecular transmetalation (Figure 1.5, Path B) [33,34].

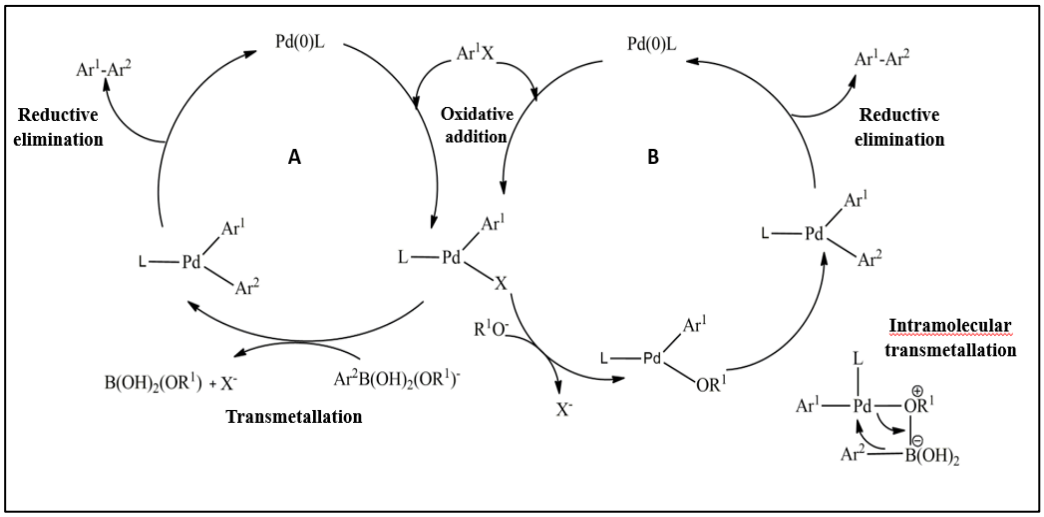

Figure 1.5. Mechanism of Suzuki polycondensation

$Pd(PPh_3)_4$ is the most common catalyst source in Suzuki reaction. Reaction is conducted in a two phase solvent mixture with organic solvents and aqueous medium for the base. As organic solvents toluene, THF or dioxane can be used and frequently used bases are K_3PO_4, K_2CO_3, KOH, Na_2CO_3 [35].

Suzuki reaction offers mild reaction conditions and tolerable to the wide range of functional groups. However, due to the basic reaction conditions compounds that are sensitive or instable in basic medium cannot be synthesized via Suzuki coupling. Commercial availability and non-toxic nature of organoboronic compounds are important features for the preference of Suzuki reaction [32,36].

1.5. Organic Solar Cells

Renewable energy sources such as wind, water or solar radiation are continuous and environmentally available sources that have potential to be replaced with traditional energy suppliers. In order to obtain electricity directly from solar light photovoltaic devices are constructed and much effort has been exerted in recent years to develop new technologies and low-cost solar cell devices. Semiconductor materials are employed in active (light-harvesting) layer of photovoltaic devices and they can be

either inorganic or organic materials. Mostly used solar cells are inorganic types due to their higher efficiencies over organic ones resulting from their higher charge carrier mobility and crystalline structures. However high production cost of inorganic solar cells leads current research to improve efficiencies of organic solar cells. Organic semiconductors provide low-cost, solution processability, high absorption coefficients, flexibility over their inorganic counterparts. Conjugated polymers have drawn considerable interest in this area and research have been proceeding to overcome low efficiency issue via structural modification of polymers using synthetic methods [37,38].

1.5.1. Working Principle of Organic Solar Cells

Organic solar cells operate to produce electricity from solar radiation with successive four step process;

1.Exciton generation by absorption of sunlight

2. Exciton diffusion to an interface

3. Charge separation

4.Charge collection at the respective electrodes (Figure 1.6)

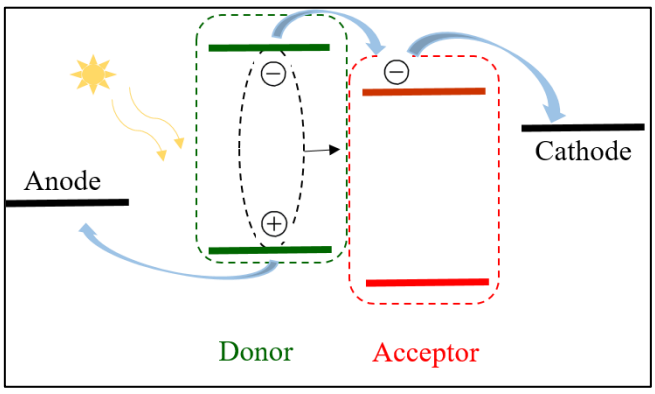

Figure 1.6. Working principle of organic solar cell

In organic photovoltaics light is absorbed by the active layer inside the device to excite an electron from HOMO to LUMO of polymer. Instead of forming free charge carriers, in organic photovoltaics excitons are created with the light absorption. Excitons are electron-hole pairs which are tightly bound with Coulomb interactions. Exciton diffusion to an interface, donor-acceptor interface in case of bulk-heterojunction type devices, is followed by the exciton dissociation to generate free charge carriers. After charge separation, as a final route, holes are transported to high work function electrode (anode) and electrons are transported to low work function electrode (cathode) for the creation of electricity [39,40].

Since the electricity generation of organic photovoltaics starts with the absorption of solar light, effective absorption is a significant parameter for the efficiency of the device. Effective absorption is achieved by active layer if the optical band gap of the polymer suits with the solar spectrum therefore utilization of high band gap polymers results in lower efficiencies for organic solar cells. Exciton diffusion length is an important feature for the efficiency of organic photovoltaics as well. Whether or not the exciton diffuses to the dissociation interface in the active layer is determined by this diffusion length which is around 10 nm for organic semiconductors. However active layer thickness should be around 100 nm for the absorption of sufficient photons therefore only the photons absorbed in the range of exciton diffusion length can reach to the interface leading loss of photons absorbed out of this range. Charge transport to the electrodes after exciton dissociation must be completed within the lifetimes of excitons for increased efficiency for organic photovoltaics [39,41].

When the process of electric generation and parameters in each step is considered different reasons are possible for energy loss in organic photovoltaic devices. Due to the limitations of high band gap and thickness of active layer, absorption losses are encountered. When dissociation interface exceeds the exciton diffusion length exciton decay is observed creating power loss. In case of recombination of electron and hole pair, charge transport to electrodes is negatively affected and efficiency of device is lowered [42].

1.5.2. Device Architectures for Organic Solar Cells

As a general structure in most of organic solar cell architectures, active layer is placed between two different electrodes. One of the electrodes which is the anode has a high work function to collect holes and other one, the cathode, has a low work function to collect electrons. As anode indium-tin oxide (ITO) is extensively used due to its transparent property and as cathode low work function metals like Al, Ca, Mg can be used [40]. In order to increase power conversion efficiency of the operating device different architectures have been developed over the years. Starting from single layer, bilayer and bulk-heterojunction type devices have been constructed.

1.5.2.1. Single Layer Organic Solar Cells

At the beginning organic solar cells were constructed with simple single layer device structure consisting organic semiconductor active layer and two electrodes (Figure 1.7). Even though they provide easy fabrication, efficiency of the devices is not high. Recombination of electron hole pair before reaching electrodes is highly probable since both electrons and holes travel in a single electro active layer. Due to small exciton diffusion length all the photons absorbed in the active layer do not contribute to the efficiency of the device. In addition, the energy supplied for exciton dissociation is not sufficient in single layer devices hence, low efficiencies are also resulted from ineffective charge separation [39,43].

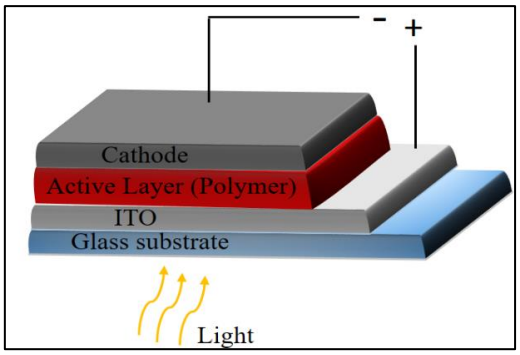

Figure 1.7. Single layer device architecture

1.5.2.2. Bilayer Organic Solar Cells

Bilayer organic solar cells are constructed with a donor and an acceptor material on top of each other and placed between different electrodes (Figure 1.8), as first proposed by Tang in 1986 [44]. The purpose in bilayer device architecture is to create donor-acceptor heterojunction to facilitate exciton dissociation for better efficiency. Because of the difference between ionization potential and electron affinity of donor and acceptor, large potential change is observed at donor-acceptor interface which provides efficient charge separation for the exciton. Therefore, exciton dissociation is more favorable in bilayer organic solar cells than their single layer counterparts. After improved exciton dissociation the free charge carriers have possibility to travel through different materials. Electrons can travel through acceptor material and holes can travel through donor material and this situation causes decrease in recombination resulting better efficiency. Even though bilayer organic solar cells are advantageous over single layer organic solar cells, they also suffer from few drawbacks. Exciton diffusion length limits the use of all absorbed photons in bilayer devices as well because photons absorbed far from donor-acceptor interface in the active layer are lost causing decreased efficiency. In addition, donor-acceptor interface area is not large enough which leads to lower efficiencies [43,45,46].

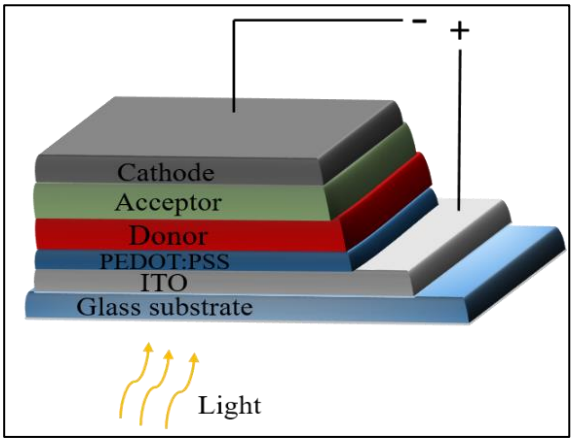

Figure 1.8. Bilayer device architecture

1.5.2.3. Bulk-Heterojunction Organic Solar Cells

Bulk heterojunction device architecture resembles bilayer structure in terms of using both donor and acceptor materials to create interface for exciton dissociation. However, in bulk heterojunction type of photovoltaic device donor-acceptor interfacial area is significantly increased allowing much more efficient charge separation than bilayer devices. Extended interfacial area is the outcome of blending donor and acceptor materials to form an interpenetrating network (Figure 1.9). In bulk heterojunction devices donor-acceptor interfaces are dispersed through the active layer and they are at sufficient length scale required for exciton diffusion. Hence all excitons generated in the active layer have possibility to easily migrate to the donor-acceptor interface and to dissociate into electrons and holes [47–49]. Energy loss due to recombination is also lowered in bulk heterojunction devices because dissociated charges can be transported to the electrodes through separate phases; electrons through acceptor and holes through donor [50]. As donor materials semiconductor conjugated polymers are used and as acceptor fullerene derivatives are extensively used due to their good electronic properties [51].

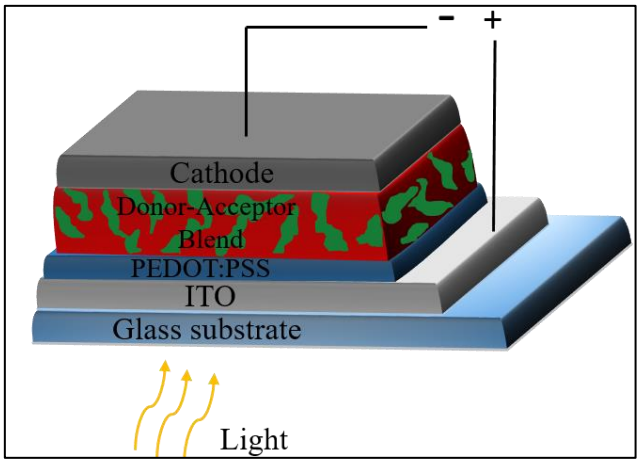

Figure 1.9. Bulk-heterojunction device architecture

1.5.3. Characteristics of Organic Solar Cells

Main goal in organic solar cells that has been pursued in recent years is to enhance power conversion efficiencies of the devices to be comparable with inorganic photovoltaics. Research area on both structural modifications of conductive polymers and employment of different device architectures has been contributing to increase in power conversion efficiency of organic solar cells. Power conversion efficiency (PCE) is the measure of power generated by the solar cell relative to the incident solar light, P_{in}. PCE of a solar cell depends on different parameters like V_{oc}, J_{sc} and fill factor (FF) and these are used to characterize the solar cells. Dependence of PCE on these parameters is formulated as below [52].

$$PCE\ (\eta_e) = P_{out} / P_{in} = (FF * V_{oc} * J_{sc}) / P_{in}$$

1.5.3.1. Open Circuit Voltage, V_{oc}

V_{oc} is described as the maximum voltage for the solar cell due to the potential difference between two electrodes when there is no flow of current under solar radiation. V_{oc} of a solar cell depends highly on the energy difference between highest occupied molecular orbital (HOMO) of the donor material and lowest occupied molecular orbital (LOMO) of acceptor material [52,53]. V_{oc} was expressed by an empirical formula in 2006, demonstrating the relation of donor HOMO and acceptor LUMO [54].

$$V_{oc} = (1/e)\ (|E, HOMO^{Donor}| - |E, LOMO^{Acceptor}|) - 0.3\ V$$

In the formulation e represents elementary charge and 0.3 V is a practically determined value for V_{oc} loss.

1.5.3.2. Short Circuit Current, J_{sc}

Maximum producible current by the organic solar device is defined as short circuit current. J_{sc} is the current flow when the device is in short-circuited state under solar light and at zero potential [52]. Short circuit current supplies information about the device in different terms. Effective light absorption, exciton dissociation and charge collection are the factors influences the $J_{sc.}$ Therefore, short circuit current is an important characteristic of an organic solar cell for increased power conversion efficiency [55].

1.5.3.3. Fill Factor, FF

For measuring of power conversion efficiency of a solar cell fill factor plays an important role. In a current (J) vs. voltage (V) curve of a solar cell device as shown in Figure 1.10 features determining the characteristics of a solar cell are depicted. When illuminated with solar radiation, solar cell device generates a maximum point on J-V graph where both current and voltage are maximized and product of these values gives the maximum power. Fill factor is the ratio of this maximum power to the product of V_{oc} and J_{sc} which are the theoretical maximum voltage and current for solar cell. As the J-V curve approaches to square shape power increases as a consequence. Fill factor represents the closeness to this square area for the operating device. FF is formulated as given below [56,57].

$FF= (J_{mp} * V_{mp})/ (J_{sc} * V_{oc})$

For fill factor to be increased charge dissociation and charge transport through the active layer should be effective and recombination loss should be less. High fill factor and high J_{sc} and therefore highly efficient solar cell can be attained with improvements in active layer morphology [58].

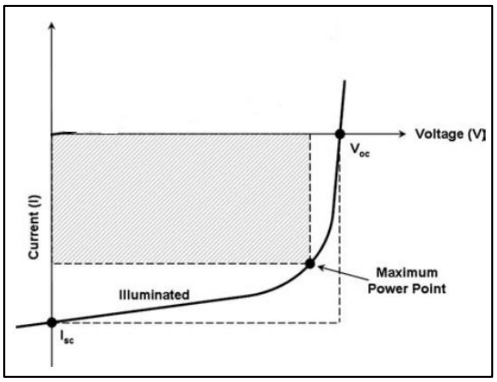

Figure 1.10. J-V curve of organic solar cell under illumination [52]

1.5.4. Recent Advances in Power Conversion Efficiency

Research on improving power conversion efficiency of solar cells has been proceeding in both device construction and conducting polymer modifications. High efficiency organic photovoltaic devices have been developed in very recent years. For example, in 2011 Chu *et al.* have synthesized a copolymer bearing dithienosilole and thieno pyrrole-4,6-dione units and reached to 7.3 % PCE with fill factor of 0.68 [59]. In 2013, alternating copolymer synthesized by Zhang *et al.* have exhibited 8.07 % power conversion efficiency with bulk-heterojunction solar cell [60].

First organic solar cell that has power conversion efficiency more than 10 % has been reported by You *et al.* in 2013 [61]. Here, with conventional device structure of polymer-fullerene blend, they have obtained 7.9 % PCE. However, when they have employed tandem solar cell device architecture, which enables more absorption of solar radiation [62], the PCE of the device has increased to 10.6 %. In 2015, power conversion efficiency of 11.3 % have been attained by Zhou *et al.* again with tandem device architecture [63].

1.6. Naphthodithiophene Moiety

Naphthodithiophene (NDT) is a thiophene fused naphthalene unit which is a good candidate for donor acceptor type polymers as the donor moiety. Naphthodithiophene is an analogue to benzodithiophene unit which is widely used donor molecule offering high power conversion efficiencies in solar cell application. It has a rigid and planar structure and provides extended π-conjugation when incorporated into polymer backbone. Due to high charge carrier property and strong intermolecular interactions, naphthodithiophene unit has drawn considerable interest for the synthesis of conjugated polymers. Naphthodithiophene is mostly used in organic field effect transistors but recently it has been used in organic photovoltaics as well. However, synthesis of NDT units requires too much effort since it suffers from the absence of practical synthetic routes. Synthetic difficulty makes naphthodithiophene unit less popular than its analogue, benzodithiophene. Therefore, its utilization in organic solar cells is limited. There are different structural isomers of naphthodithiophene unit demonstrated in Figure 1.11 [64–66].

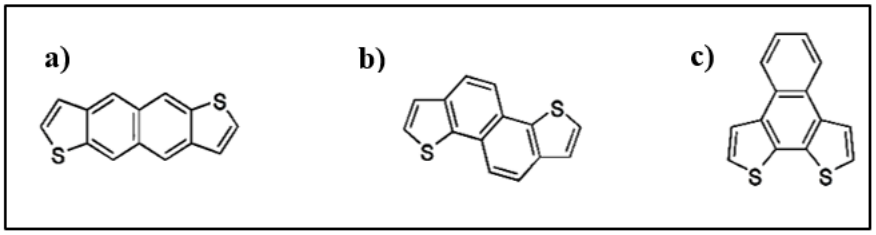

Figure 1.11. Structural isomers of NDT

1.6.1. Naphtho[2,3-*b*:6,7-*b'*]dithiophene

This isomer of naphthodithiophene is commonly referred as linear NDT. First use of naphthodithiophene unit in organic solar cells was achieved with linear NDT in 2011 by Marks and co-workers. Instead of using polymeric semiconductor they synthesized a small molecule from linear NDT and diketopyrrolopyrrole as the donor material in solar cells (Figure 1.12). Since the rigid structure of naphthodithiophene

unit is lack of solubility, NDT was functionalized with alkoxy groups to obtain soluble molecule. Linear NDT based organic solar cell device reached to 4.06 % power conversion efficiency due to its ordered molecular structure and high hole mobility [67].

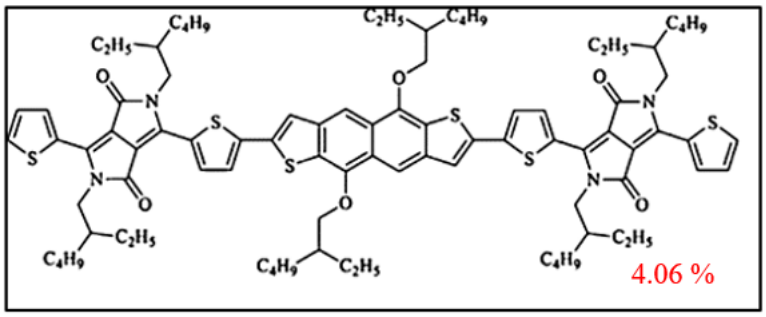

Figure 1.12. Structure of linear NDT based small molecule

In 2012, linear NDT was again combined with diketopyrrolopyrrole unit but copolymer of these two units was synthesized rather than a small molecule by Peng *et al.* This is the first report of using NDT based copolymer used as an active layer in organic photovoltaics which has 5.37 % efficiency [68]. Structure of the polymer is shown in Figure 1.13,a. Later on in 2012, Lee and co-workers developed a novel polymer bearing linear NDT and thieno-pyrrole-4,6-dione (Figure 1.13,b) and used in organic solar cell to obtain 4.0 % efficiency device [69]. Another linear NDT based polymer was synthesized by Lee and co-workers in 2013 which comprises fluorine substituted thienothiophene unit (Figure 1.13,c). Power conversion efficiency of 5.16 % was achieved with this donor in organic photovoltaics [70].

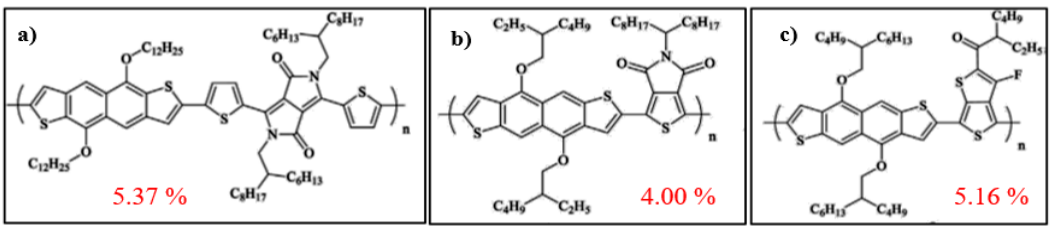

Figure 1.13. Structures of linear NDT based conjugated polymers

1.6.2. Naphtho[1,2-*b*:5,6-*b'*]dithiophene

1.6.2.1. Unsubstituted Naphtho[1,2-*b*:5,6-*b'*]dithiophene

After the implementations of linear NDT to organic photovoltaics a new 'zigzag' isomer of naphthodithiophene was suggested by Lee and co-workers in 2012. They synthesized small molecules bearing zigzag NDT and benzothiadiazole unit. The zigzag NDT core utilized had no substitution. When the small molecule was capped with triphenylamine moiety as depicted in Figure 1.14, efficiency of organic solar cell increased from 0.98 % to 2.20 % which was the highest value for this device. The increase in the efficiency was the result of enhanced conjugation and absorption [71].

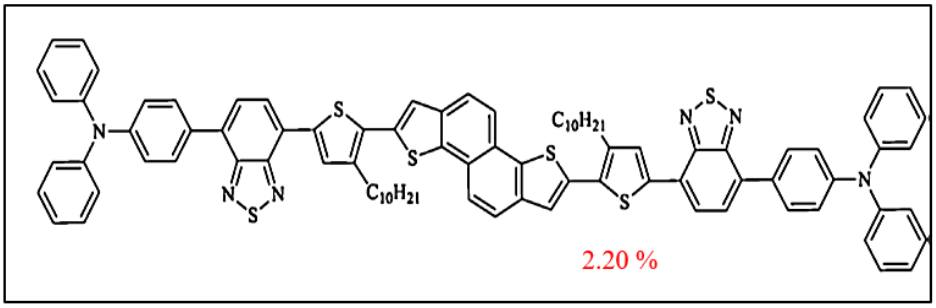

Figure 1.14. Zigzag NDT based small molecule

Takimiya and co-workers synthesized two different polymers bearing zigzag NDT in the polymer backbone to be used in both organic photovoltaics and organic field effect transistors. They used benzothiadiazole and naphthobisthiadiazole as electron deficient groups in donor-acceptor type polymers (Figure 1.15). Switching from benzothiadiazole to naphthobisthiadiazole power conversion efficiency of the corresponding devices increased from 3.8 % to 4.9 % due to enhancement in the π electron system [72].

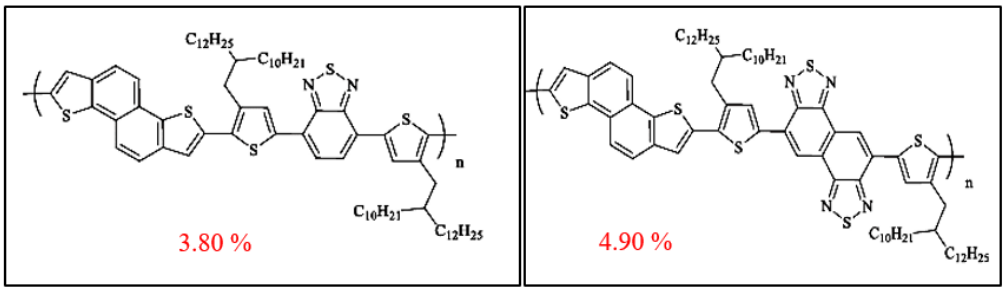

Figure 1.15. Zigzag NDT, benzothiadiazole and naphthobisthiadiazole based copolymers

In 2004 again Lee and co-workers synthesized and characterized three different conjugated polymers bearing unsubstituted zigzag NDT unit with quinoxaline moieties [73]. Highest efficiency of 1.61% was obtained with polymer demonstrated in Figure 1.16.

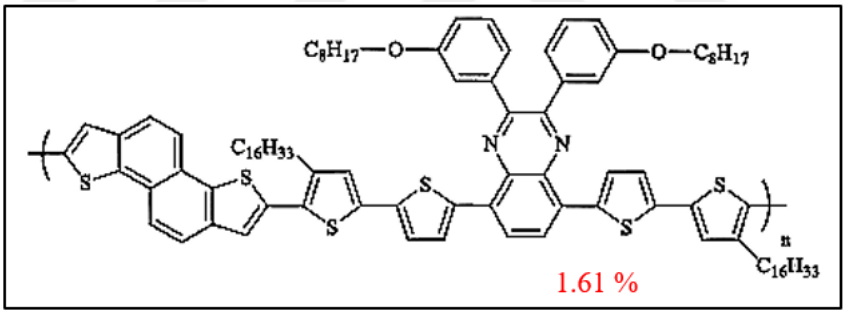

Figure 1.16. Structure of Z-NDT and quinoxaline bearing copolymer

1.6.2.2. Alkoxy- Substituted Naphtho[1,2-*b*:5,6-*b'*]dithiophene

In order to facilitate the solubility of zigzag NDT bearing polymers, alkoxy groups were introduced to the NDT core first time by Li and co-workers in 2013. They synthesized a Z-NDT and thieno-pyrrole-4,6-dione bearing alternating copolymer (Figure 1.17, a) in which broad band gap polymer was obtained and 5.30% PCE has been achieved [74]. Later on, same group synthesized two different polymers bearing

benzothiadiazole and benzooxadiazole units as acceptor molecules in the polymer backbone (Figure 1.17, b). Highest efficiency in photovoltaic devices was attained with benzooxadiazole bearing conjugated polymer with a value of 5.07 % due to the strong electron acceptor nature of benzooxadiazole which elevates intramolecular charge transfer [75]. In 2013, Lee and co-workers synthesized a copolymer combining zigzag NDT and fluorine substituted thienothiophene unit (Figure 1.17, c). Photovoltaic device of this polymer displayed 4.88% power conversion efficiency which is lower than that of linear NDT bearing polymer [76].

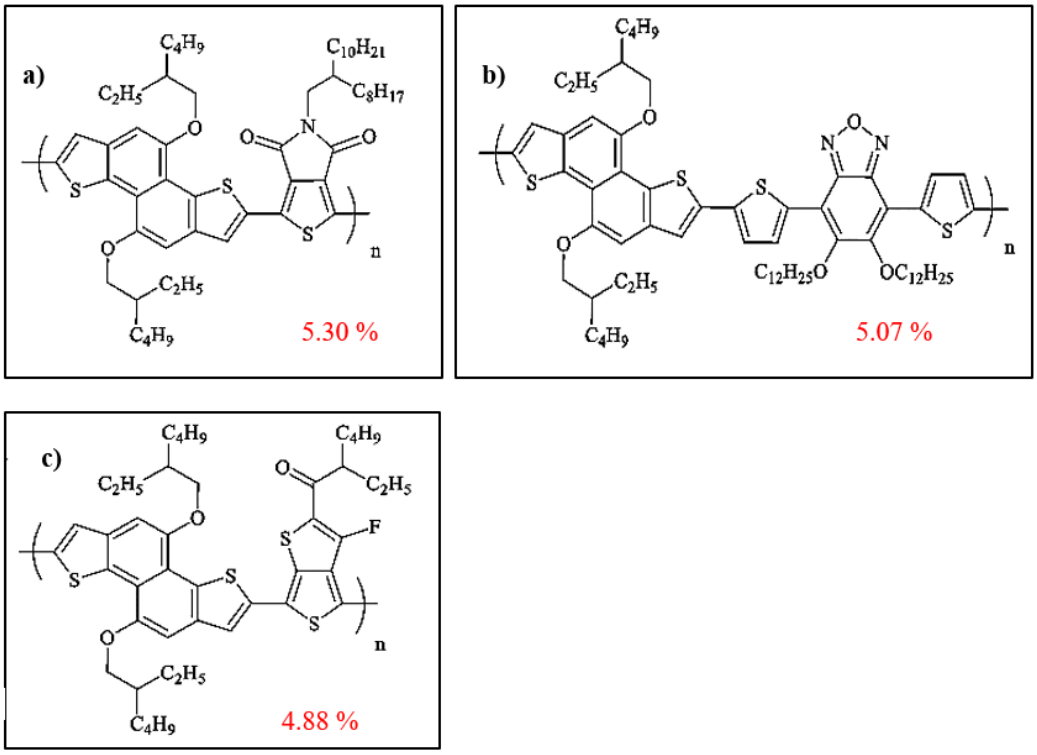

Figure 1.17. Structures of alkoxy functionalized Z-NDT based copolymers

1.6.2.3. Alkyl- Substituted Naphtho[1,2-*b*:5,6-*b'*]dithiophene

As an alternative to enhance solubility of the polymers, zigzag NDT core can be functionalized with alkyl groups as well. In 2013 Takimiya and co-workers utilized alkyl functionalized zigzag NDT as donor and naphthobisthiadiazole as acceptor in the

polymer backbone (Figure 1.18, a). They reached to power conversion efficiency of 8.20 % which is much higher than other NDT bearing donor molecules. Introduction of alkyl chains rather than alkoxy groups improved orientation of molecules to yield better results in solar cells [77]. Recently, Cheng *et al.* synthesized branched-alkyl chain functionalized NDT bearing polymer demonstrating 6.86 % power conversion efficiency in photovoltaic devices (Figure 1.18,b) [78].

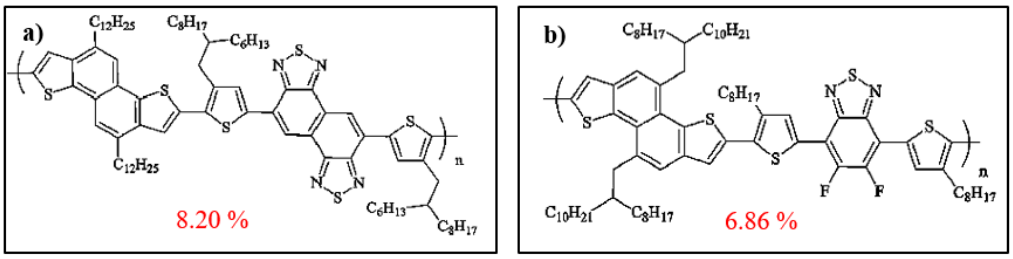

Figure 1.18. Structures of alkyl functionalized Z-NDT based copolymers

1.6.2. Naphtho[2,3-*b*:3,4-*b'*]dithiophene

Naphtho[2,3-*b*:3,4-*b'*]dithiophene is another structural isomer of NDT which was synthesized in 2008 with alkyl substituents to improve solubility of the resulting polymer by You and co-workers. NDT and cyclopentadithiophene bearing alternating copolymer was synthesized and organic solar cell has been constructed (Figure 1.19, a). Power conversion efficiency of 0.55 % have been observed with a broad band gap polymer since both units have electron rich character [79]. Later, in 2011 two new polymers comprising NDT and thionethiophene and fluorine substituted thiohethiophene have been synthesized by same group (Figure 1.19, b) which displayed 0.43 % and 0.46 % power conversion efficiencies respectively. These low PCEs arise from lower molecular weight and low hole mobility of polymers [80].

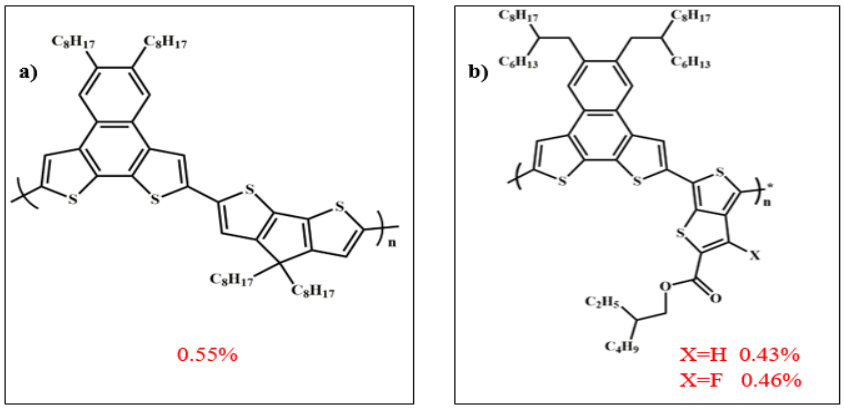

Figure 1.19. Alkyl substituted Naphtho[2,3-b:3,4-b']dithiophene based copolymers

In 2011, NDT core was functionalized with alkoxy groups by Wang *et al*. with benzothiadiazole used as an acceptor moiety in the polymer backbone (Figure 1.20). When compared with alkyl substituted NDT bearing polymers, these new ones revealed higher power conversion efficiencies of 0.62% and 5.27% when 1,8-Diiodooctane, DIO, was used as additive in organic solar cell applications. Enhanced efficiency in power was attributed to improved solubility and better nanoscale separation of donor-acceptor in active layer [81].

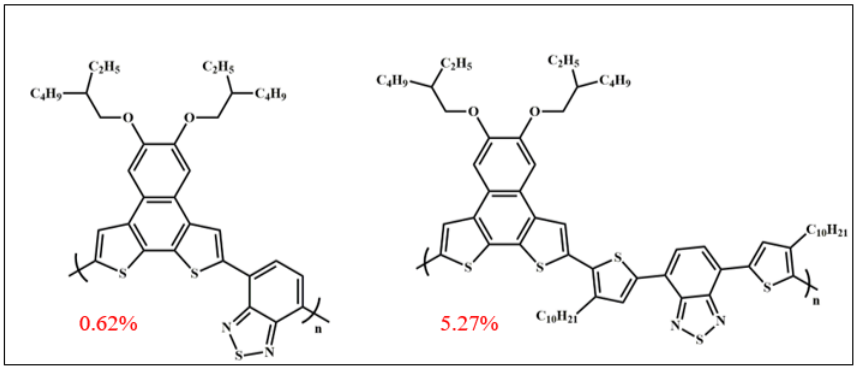

Figure 1.20. Alkoxy functionalized Naphtho[2,3-b:3,4-b']dithiophene based copolymers

Alkoxy functionalized NDT core was also used by Kim *et al.* in 2013 in three different polymers where conjugation was altered with incorporation of thiophene, terthiophene and dithiophene ethene (Figure 1.21). Power conversion efficiencies of 1.18%, 3.3% and 3.5% were found revealing that the increase of conjugation length enhances short-circuit current [82].

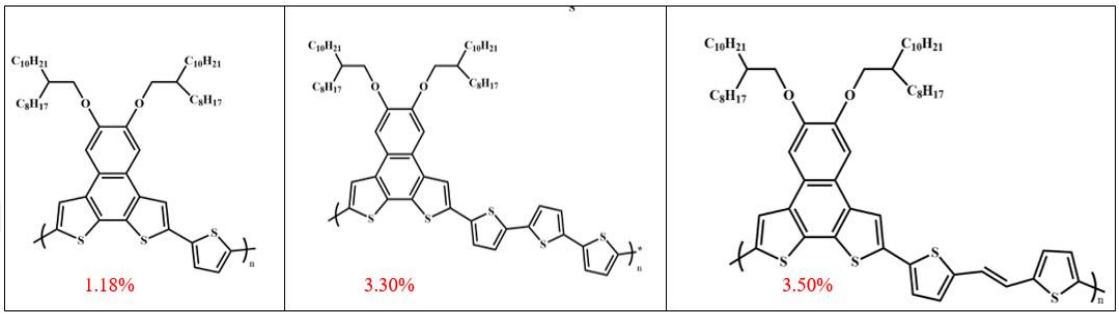

Figure 1.21. Naphtho[2,3-b:3,4-b']dithiophene based copolymers

1.7. Aim of the Study

In this study naphtho[2,3-*b*:3,4-*b'*]dithiophene unit bearing donor-acceptor type of random copolymers were designed and synthesized. NDT was suited as the donor moiety in the polymer due to its properties like having extended π-conjugation, rigid and planar structure and having high charge carrier capability. It was aimed in this study to take advantage of these properties of NDT unit in the polymer backbone for the bulk-heterojunction solar cell applications. Isomer choice of NDT relies on the synthetic pathways. Even though synthetic route to naphtho[2,3-*b*:3,4-*b'*]dithiophene required many optimizations during this study, it is relatively more facile than the synthesis of other isomers. Since solubility of the resulting polymers is an important parameter for solar cell application, dodecyloxy groups were introduced to NDT unit to have improved solubility. As acceptor unit diimine bearing benzotriazole moiety was employed due to its electron deficient nature. Also benzotriazole moiety can be functionalized with several alkyl chains to gain better solubility. Combination of NDT

and BTz moieties in the same polymer backbone was missing in the literature hence our aim was to investigate their electrochemical, spectroelectrochemical and optical properties of polymers comprising these groups. Moreover, in order to investigate the effect of increasing conjugation length in the polymer backbone thiophene and bithiophene units were used in the synthesis of polymers. Electrochemical, spectroelectrochemical and optical characterizations of synthesized random copolymers were performed to be used in the bulk-heterojunction solar cell applications.

CHAPTER 2

EXPERIMENTAL

2.1. Materials

All chemicals were purchased from Sigma-Aldrich and used without any purification in the synthesis and characterizations of polymers. THF and toluene were freshly distilled from Na-benzophenone ketyl before usage to obtain dry solvents. Merck Silica Gel 60 was used in column chromatography for the purification process. 4,7-bis(5-bromothiophen-2-yl)-2-dodecyl-2H-benzo[*d*][1,2,3]triazole was synthesized accordingly with literature [83] and 5,6-bis(dodecyloxy)naphtho[2,1-*b*:3,4-*b'*]dithiophene was synthesized with modification in previously described procedures [79,84].

2.2. Equipments

Structural characterization of compounds was performed with ^{1}H and ^{13}C NMR spectra which were recorded with Bruker Spectrospin Avance DPX-400 Spectrometer. All chemical shifts were in ppm according to tetramethylsilane (TMS) as internal reference and $CDCl_3$ as solvent. High Resolution Mass Spectroscopy measurements were carried out with Waters Synapt MS system. Gel Permeation Chromatography (GPC) was utilized in order to determine the average molecular weights and polydispersity index of polymers with Shimadzu GPC, with polystyrene standards where chloroform was the choice of eluent. Electrochemical studies were conducted by GAMRY Reference 600 Potentiostat with a three-electrode cell system containing indium tin oxide (ITO) coated glass as the working electrode, Pt wire as the counter electrode and Ag wire as the reference electrode in

0.1 M solution of tetrabutylammonium hexafluorophosphate-acetonitrile (ACN). HOMO and LUMO energy levels of polymers were calculated taking NHE as -4.75 eV with respect to vacuum. Spectroelectrochemical characterization of the polymers were completed with Varian Cary 5000 UV-Vis-NIR Spectrophotometer. Organic solar cells were fabricated in a nitrogen gas filled glove-box system and J-V curves were recorded under AM 1.5 G simulated illumination (100mW/cm^2) with Keithley 2400 source meter. Oriel Quantum Efficiency Measurement was used for IPCE measurements.

2.3. Syntheses of Monomers

2.3.1. General Synthetic Route to Monomers

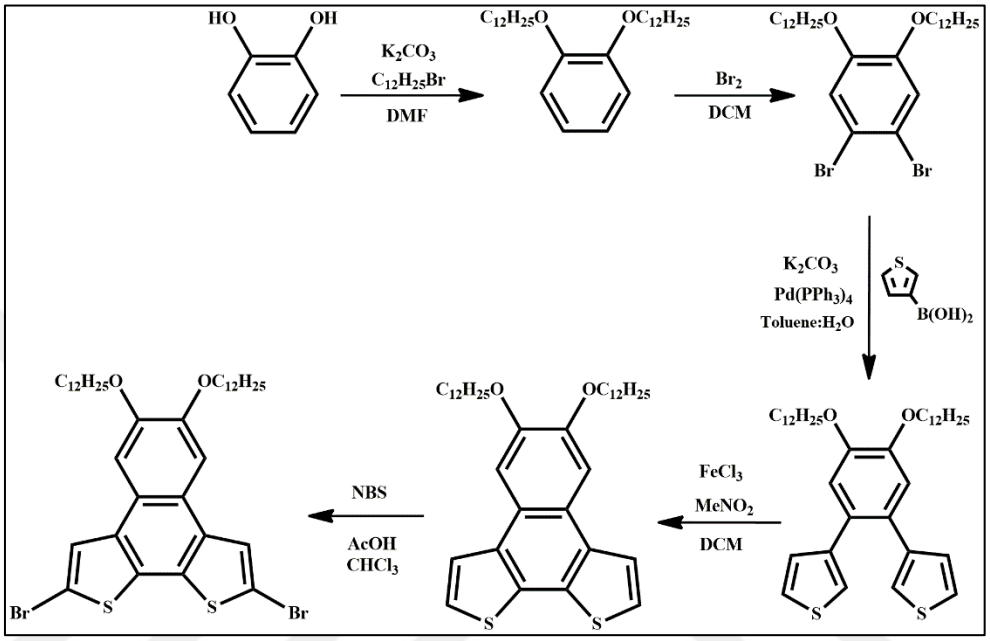

Figure 2.1. Synthetic route to NDT

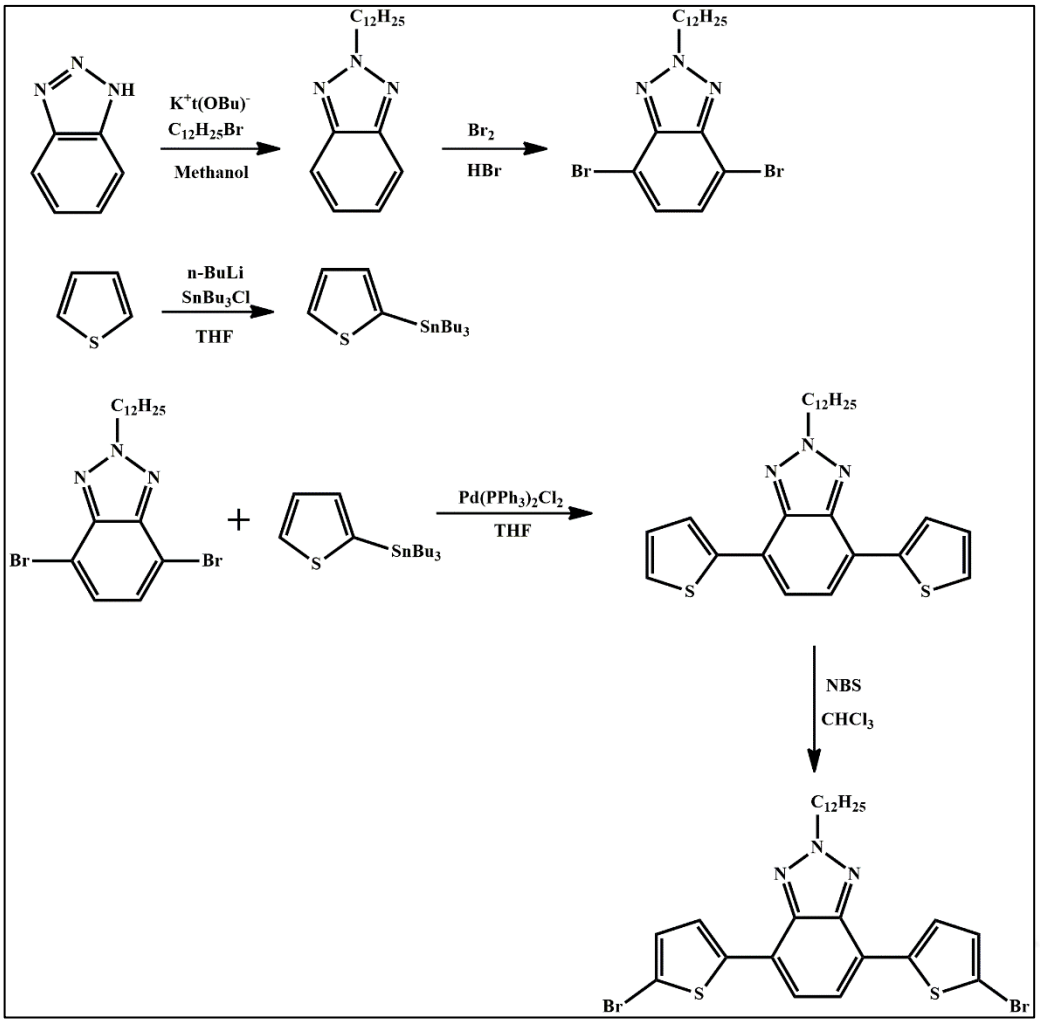

Figure 2.2. Synthetic route to TBT

2.3.2. Synthesis of 2-dodecyl-2H-benzo[*d*][1,2,3]triazole

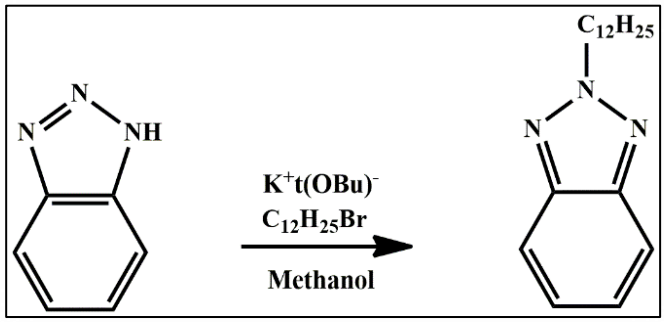

Figure 2.3. Synthetic route for 2-dodecyl-2H-benzo[*d*][1,2,3]triazole

1H-benzo[*d*][1,2,3]triazole (5.00 g, 41.9 mmol) was dissolved in methanol (40 mL) in a three neck round-bottom flask. Then, $K^+t(OBu)^-$ (5.00 g, 44.6 mmol) and 1-bromododecane (12 mL, 50 mmol) were added to the flask and resulting mixture was refluxed overnight. After the completion of reaction, methanol was evaporated under reduced pressure and residue was dissolved in $CHCl_3$ and washed with water. Organic phase was dried over $MgSO_4$ and the solvent was evaporated. Purification was achieved with column chromatography on silica gel (2:1 DCM: Hexane) to obtain titled product as a colorless oil with 32 % yield.

^{1}H NMR (400 MHz, $CDCl_3$): δ 7.85 (m, 2H), 7.36 (m, 2H), 4.72 (t, *J*= 7.21 Hz, 2H), 2.11 (quin, *J*= 7.33 Hz, 2H), 1.23-1.34 (m, 18H), 0.87 (t, *J*= 6.70 Hz, 3H)

^{13}C NMR (100 MHz, $CDCl_3$): δ 144.27, 126.12, 117.94, 56.66, 31.90, 30.07, 29.59, 29.50, 29.36, 29.31, 29.02, 26.56, 22.67, 16.61, 14.10

2.3.3. 4,7-Dibromo-2-dodecyl-2H-benzo[*d*][1,2,3]triazole

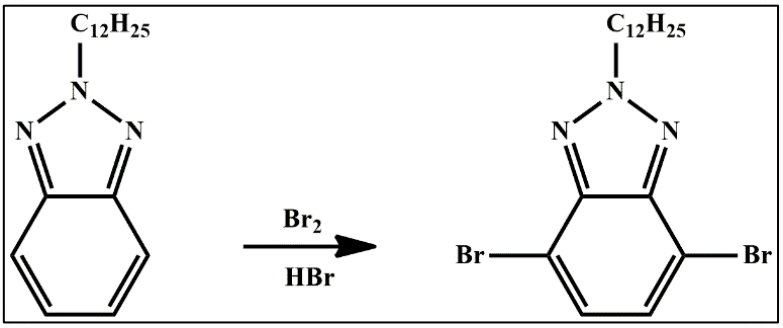

Figure 2.4. Synthetic route for 4,7-dibromo-2-dodecyl-2H-benzo[*d*][1,2,3]triazole

2-Dodecyl-2H-benzo[*d*][1,2,3]triazole (3.00 g, 10.6 mmol) and aqueous HBr (48 %, 13 mL) were put into a three neck round-bottom flask and stirred at 100 ºC for 1 hour. Then bromine (1.5 mL, 29 mmol) was added to the reaction mixture and refluxed at 135 ºC overnight. When the reaction was completed, it was allowed to cool to room temperature and a saturated $NaHCO_3$ solution was added to the reaction mixture. The product was extracted with $CHCl_3$, organic layer was separated, dried over $MgSO_4$ and solvent was removed by rotary evaporation. Column chromatography on silica gel (5:1 DCM: Hexane) was performed to obtain product as a white solid with 81% yield.

^{1}H NMR (400 MHz, $CDCl_3$): δ 7.44 (s, 2H), 4.77 (t, *J*= 7.50 Hz, 2H), 2.14 (quin, *J*= 7.34 Hz, 2H), 1.24-1.42 (m, 18H), 0.87 (t, *J*= 6.67 Hz, 3H)

^{13}C NMR (100 MHz, $CDCl_3$): δ 143.73, 129.51, 109.99, 57.49, 31.91, 30.23, 29.59, 29.49, 29.34, 28.98, 27.83, 26.51, 25.32, 22.68, 14.11

2.3.4. Synthesis of tributyl(thiophen-2-yl) stannane

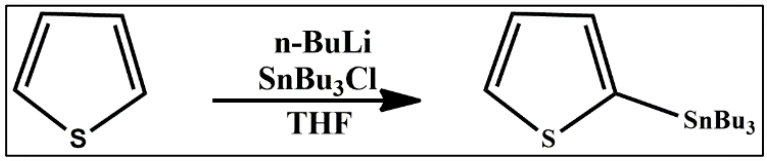

Figure 2.5. Synthetic route for tributyl(thiophen-2-yl) stannane

Thiophene (2.00 g, 23.8 mmol) and anhydrous THF (28 mL) were added to a three neck round-bottom flask under argon atmosphere. After the temperature was cooled down to -78 ºC by dry ice/acetone mixture, n-butyl lithium (2.5 M in hexane, 11.3 mL, 28.2 mmol) was added drop wise to the reaction mixture. After completion of addition, the resulting mixture was stirred at the same temperature under Ar for 1.5 hours and then tributyltin chloride (7.8 mL, 28.7 mmol) was added drop wise. The reaction mixture was stirred at -78 ºC for 4 hours and then allowed to warm to room temperature and stirred overnight. THF was evaporated under vacuum, the crude product was dissolved in chloroform and washed with saturated NH_4Cl (x2), brine and distilled water. Organic layer was dried with $MgSO_4$ and concentrated with rotary evaporator to obtain light yellow liquid with 88% yield. The product was used without further purification.

^{1}H NMR (400 MHz, $CDCl_3$): δ 7.67 (d, *J*= 4.78 Hz, 1H), 7.28 (t, *J*= 3.22 Hz, 1H), 7.21 (d, *J*= 3.15 Hz, 1H), 1.58 (m, 6H), 1.31-1.40 (m, 6H), 1.12 (t, *J*= 8.29 Hz, 6H), 0.91 (t, *J*= 7.29 Hz, 9H)

^{13}C NMR (100 MHz, $CDCl_3$): δ 136.18, 135.18, 130.58, 127.83, 28.98, 27.28, 13.68, 10.82

2.3.5. Synthesis of 2-dodecyl-4,7-di(thiophen-2-yl)-2H-benzo[*d*][1,2,3]triazole

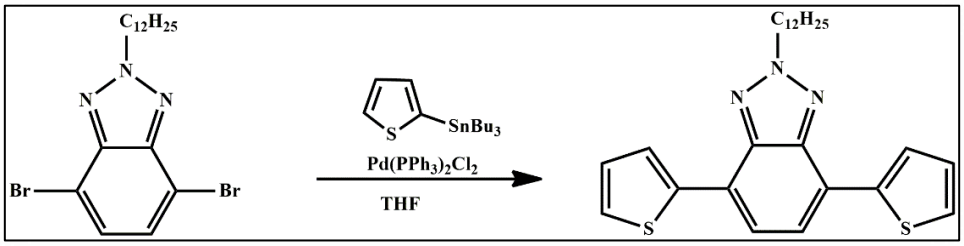

Figure 2.6. Synthetic route for 2-dodecyl-4,7-di(thiophen-2-yl)-2H-benzo[*d*][1,2,3]triazole

4,7-Dibromo-2-dodecyl-2H-benzo[*d*][1,2,3]triazole (750 mg, 1.68 mmol) and tributyl(thiophen-2-yl) stannane (1.9 g, 5.05 mmol) were dissolved in anhydrous THF (30 mL) under argon atmosphere. Dichlorobis(triphenylphopphine)-palladium(II) (70 mg, 0.099 mmol) was added to the reaction mixture and the resulting mixture was refluxed for 24 hours under argon. Reaction was monitored with TLC and after completion, THF was evaporated under reduced pressure. The crude product was purified with column chromatography on silica gel (2:1 Hexane: DCM) to obtain a green solid with 78% yield.

^{1}H NMR (400 MHz, $CDCl_3$): δ 7.99 (d, *J*= 3.59 Hz, 2H), 7.47 (s, 2H), 7.25 (d, *J*= 5.06 Hz, 2H), 7.06 (t, *J*=3.82, 2H), 4.66 (t, *J*= 7.22 Hz, 2H), 2.05 (quin, *J*= 7.07 Hz, 2H), 1.12-1.29 (m, 18H), 0.77 (t, *J*= 6.64 Hz, 3H)

^{13}C NMR (100 MHz, $CDCl_3$): δ 142.11, 140.03, 128.13, 127.02, 125.54, 123.60, 122.76, 58.88, 32.00, 30.13, 29.71, 29.64, 29.53, 29.44, 29.13, 26.67, 22.78, 14.23 (1 missing peak due to overlap in the alkyl chain region)

2.3.6. Synthesis of 4,7-bis(5-bromothiophen-2-yl)-2-dodecyl-2H-benzo[*d*][1,2,3]triazole

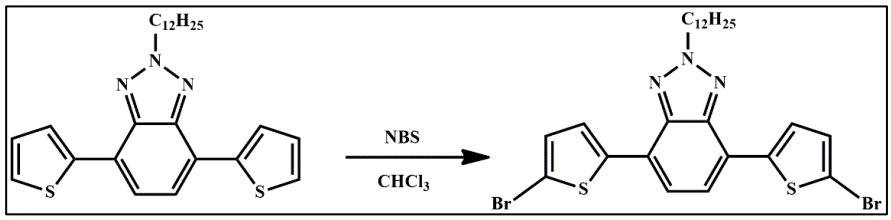

Figure 2.7. Synthesis of 4,7-bis(5-bromothiophen-2-yl)-2-dodecyl-2H-benzo[*d*][1,2,3]triazole

2-Dodecyl-4,7-di(thiophen-2-yl)-2H-benzo[*d*][1,2,3]triazole (598 mg, 1.33 mmol) was dissolved in chloroform (25 mL) at room temperature and *N*-bromosuccinimide (589 mg, 3.31 mmol) was added in portions to the reaction mixture within 2 hours. The reaction was stirred at room temperature in the dark for 24 hours. After completion of reaction, solvent was evaporated and the product was recrystallized from ethanol to give yellow solid with 86 % yield.

^{1}H NMR (400 MHz, $CDCl_3$): δ 7.79 (d, *J*= 3.95 Hz, 2H), 7.50 (s, 2H), 7.12 (d, *J*= 3.90 Hz, 2H), 4.79 (t, *J*= 7.28 Hz, 2H), 2.18 (quin, *J*= 7.46 Hz, 2H), 1.21-1.39 (m, 18H), 0.87 (t, *J*= 6.55 Hz, 3H)

^{13}C NMR (100 MHz, $CDCl_3$): δ 142.25, 130.90, 126.96, 122.23, 118.19, 115.27, 113.18, 56.96, 43.02, 31.92, 30.06, 29.63, 29.60, 29.55, 29.44, 29.35, 29.02, 22.70 (1 peak missing due to overlap in the alkyl chain region)

2.3.7. Synthesis of 1,2-bis(dodecyloxy)benzene

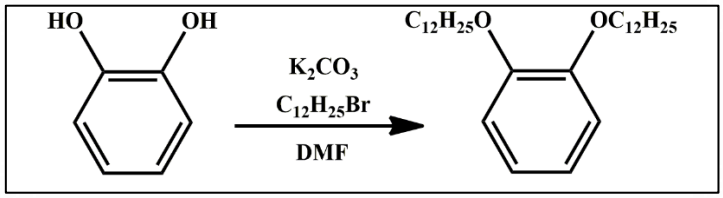

Figure 2.8. Synthetic route for 1,2-bis(dodecyloxy)benzene

Pyrocatechol (4.00 g, 36 mmol) and K_2CO_3 (14.9 g, 108mmol) were dissolved in anhydrous DMF (30 mL) at argon atmosphere. 1-Bromododecane (20.73 g, 83.2 mmol) was then added to the reaction mixture and refluxed for 40 hours under inert atmosphere. After the reaction was completed, it was cooled down to room temperature and washed with excess distilled water. The product was extracted with dichloromethane, organic layer was separated and dried with $MgSO_4$. Solvent was evaporated under vacuum and crude product was recrystallized from methanol, filtrated and washed with methanol several times to get white solid with 64% yield.

^{1}H NMR (400 MHz, $CDCl_3$): δ 6.88 (s, 4H), 3.99 (t, *J*= 6.64 Hz, 4H), 1.80 (quin, *J*= 6.78 Hz, 4H), 1.26-1.50 (m, 36H), 0.88 (t, *J*= 6.55 Hz, 6H)

^{13}C NMR (100 MHz, $CDCl_3$): δ 149.33, 121.03, 114.25, 69.34, 31.94, 29.71, 29.66, 29.48, 29.38, 26.06, 22.70, 14.10 (3 missing peaks are due to overlaps)

2.3.8. Synthesis of 1,2-dibromo-4,5-bis(dodecyloxy)benzene

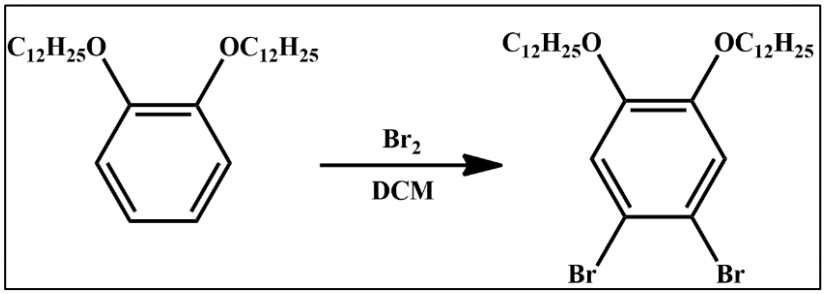

Figure 2.9. Synthetic route for 1,2-dibromo-4,5-bis(dodecyloxy)benzene

1,2-Bis(dodecyloxy)benzene (1.00 g, 2.24 mmol) was dissolved in DCM (20 mL) in a three neck round bottom flask connected to condenser with gas outlet filled with 10% aqueous NaOH solution. Bromine (0.23 mL, 4.48 mmol) in DCM (5 mL) was then added to the reaction mixture dropwise at 0 ºC. The reaction mixture was stirred under dark at room temperature overnight. Completion of reaction was monitored with TLC and into the resulting mixture saturated $NaHSO_3$ was added to remove excess bromine. The product was extracted with dichloromethane, combined organic layers were dried over $MgSO_4$ and the solvent was evaporated. Purification of crude product by column chromatography on silica gel (5:1 Hexane: DCM) was performed to obtain the product as a white solid with 79% yield.

^{1}H NMR (400 MHz, $CDCl_3$): δ 7.06 (s, 2H), 3.94 (t, *J*= 6.60 Hz, 4H), 1.79 (quin, *J*= 6.71 Hz, 4H), 1.26-1.48 (m, 36H), 0.88 (t, *J*= 6.52 Hz, 6H)

^{13}C NMR (100 MHz, $CDCl_3$): δ 149.07, 118.08, 114.67, 69.64, 31.93, 30.91, 29.69, 29.66, 29.60, 29.36, 29.34, 29.05, 25.93, 22.69, 14.11

HRMS for $C_{30}H_{52}O_2Br_2$ calculated 602.2334, found 602.2338

2.3.9. Synthesis of 3,3'-(4,5-bis(dodecyloxy)-1,2-phenylene) dithiophene

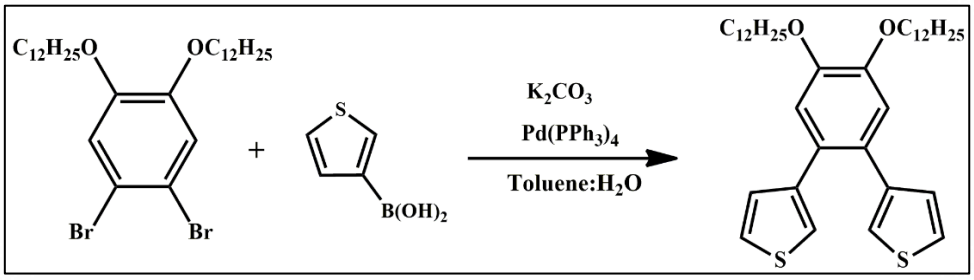

Figure 2.10. Synthetic route for 3,3'-(4,5-bis(dodecyloxy)-1,2-phenylene) dithiophene

1,2-Dibromo-4,5-bis(dodecyloxy)benzene (1.22 g, 2.01 mmol), 3-thienylboronic acid (1.03 g, 8.05 mmol) and 2M K_2CO_3 were dissolved in dry toluene (30 mL, 3:2 Toluene: H_2O) in a two neck round bottom flask. Into the reaction mixture $Pd(PPh_3)_4$ (116 mg, 0.01 mmol) and Aliquat 336 (2 drops) were added and resulting mixture was refluxed under inert atmosphere for two days. When the reaction was completed toluene was evaporated under reduced pressure, crude product was dissolved in dichloromethane and washed with water. Organic phase was dried over $MgSO_4$. After removal of the solvent, the product was purified by column chromatography on silica gel (2:1 Hexane: DCM) to give white solid with 65 % yield.

^{1}H NMR (400 MHz, $CDCl_3$): δ 7.16 (dd, *J*= 7.95, *J*= 2.99, 2H), 7.01 (dd, *J*= 4.22, *J*= 1.25, 2H), 6.95 (s, 2H), 6.76 (dd, *J*= 6.20, *J*= 1.25, 2H), 4.04 (t, *J*= 6.63 Hz, 4H), 1.83 (quin, *J*= 6.77 Hz, 4H), 1.26-1.51 (m, 36H), 0.88 (t, *J*= 6.58 Hz, 6H)

^{13}C NMR (100 MHz, $CDCl_3$): δ 148.41, 142.07, 129.11, 128.03, 124.50, 122.28, 115.83, 69.52, 31.93, 29.71, 29.65, 29.43, 29.37, 29.34, 26.05, 22.70, 14.12 (2 missing peaks are due to overlaps in the alkyl chain region)

HRMS for $C_{38}H_{58}O_2S_2$ calculated 611.3957, found 611.3969

2.3.10. Synthesis of 5,6-bis(dodecyloxy)naphtho[2,1-*b*:3,4-*b'*]dithiophene (NDT)

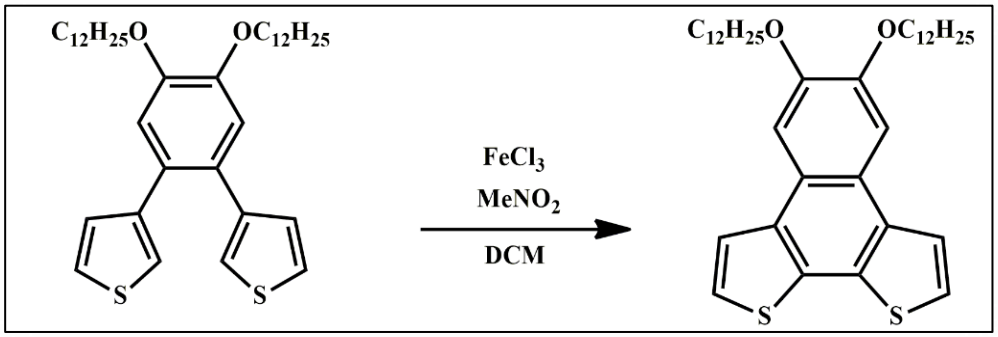

Figure 2.11. Synthetic route for 5,6-bis(dodecyloxy)naphtho[2,1-*b*:3,4-*b'*]dithiophene

3,3'-(4,5-Bis(dodecyloxy)-1,2-phenylene) dithiophene (809 mg, 1.32 mmol) was dissolved in dry DCM (40 mL) in a three neck round bottom flask. To the stirred solution, anhydrous iron(III) chloride (536 mg, 3.30 mmol) in $MeNO_2$ (10 mL) was added dropwise under argon atmosphere. After complete addition, the mixture was stirred for 1 hour at room temperature under inert atmosphere then methanol (10 mL) was added and the mixture was further stirred for 30 min. Solvent was evaporated under reduced pressure after completion of reaction, the crude product was dissolved in DCM and washed with aqueous NH_4Cl several times. Organic layer was dried over $MgSO_4$. Column chromatography on silica gel was (2:1 Hexane: $CHCl_3$) performed to obtain pale yellow solid with 57 % yield.

^{1}H NMR (400 MHz, $CDCl_3$): δ 7.87 (d, *J*= 5.37 Hz, 2H), 7.69 (s, 2H), 7.47 (d, *J*= 5.34 Hz, 2H), 4.20 (t, *J*= 6.60 Hz, 4H), 1.94 (quin, *J*= 6.76 Hz, 4H), 1.27-1.59 (m, 36H), 0.88 (t, *J*= 6.51 Hz, 6H)

^{13}C NMR (100 MHz, $CDCl_3$): δ 148.89, 133.89, 130.43, 123.45, 122.75, 122.55, 106.87, 69.30, 31.95, 29.74, 29.69, 29.51, 29.40, 29.31, 26.15, 22.72, 14.14 (2 missing peaks are due to overlaps in the alkyl chain region)

HRMS for $C_{38}H_{56}O_2S_2$ calculated 608.3722, found 608.3726

2.3.11. Synthesis of 2,9-dibromo-5,6-bis(dodecyloxy)naphtho[2,1-*b*:3,4-*b'*]dithiophene

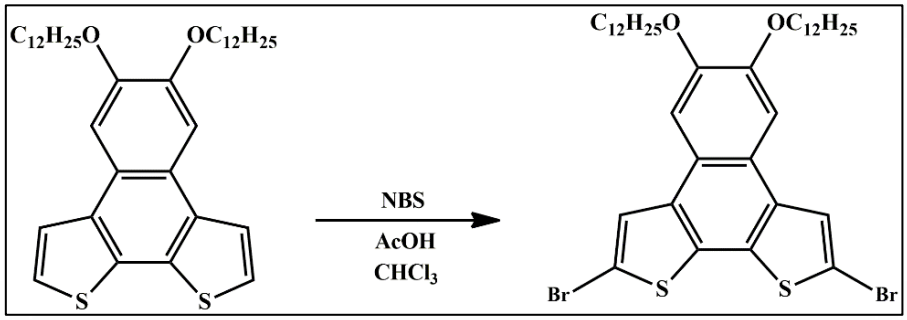

Figure 2.12. Synthetic route for 2,9-dibromo-5,6-bis(dodecyloxy)naphtho[2,1-*b*:3,4-*b'*]dithiophene

5,6-Bis(dodecyloxy)naphtho[2,1-*b*:3,4-*b'*]dithiophene (480 mg, 0.79 mmol) was dissolved in mixture of $CHCl_3$ (15 mL) and glacial acetic acid (15 mL). *N*-bromosuccinimide (308 mg, 1.73 mmol) was added in portions to the reaction mixture and stirred overnight at room temperature. The resulting mixture was poured into distilled water. The organic layer was extracted with chloroform and was washed with 5 % aqueous NaOH solution and brine. Combined organic phases were dried with $MgSO_4$ and solvent was removed under vacuum. Flash column chromatography on silica gel (5:1 Hexane: $CHCl_3$) was performed. The crude product was further purified with recrystallization from $CHCl_3$ (3 times) to obtain a white solid with 37 % yield.

^{1}H NMR (400 MHz, $CDCl_3$): δ 7.83 (s, 2H), 7.51 (s, 2H), 4.17 (t, *J*= 6.58 Hz, 4H), 1.93 (quin, *J*= 6.85 Hz, 4H), 1.26-1.43 (m, 36H), 0.88 (t, *J*= 6.62 Hz, 6H)

^{13}C NMR (100 MHz, $CDCl_3$): δ 167.09, 149.39, 133.72, 125.47, 121.80, 120.91, 112.18, 69.29, 31.93, 29.74, 29.70, 29.65, 29.46, 29.37, 29.27, 29.23, 26.10, 22.69, 14.10 (1 peak missing due to overlap in the alkyl chain region)

HRMS for $C_{38}H_{54}O_2S_2Br_2$ calculated 765.2010, found 765.2046

2.4. Syntheses of Polymers

2.4.1. Synthesis of P1

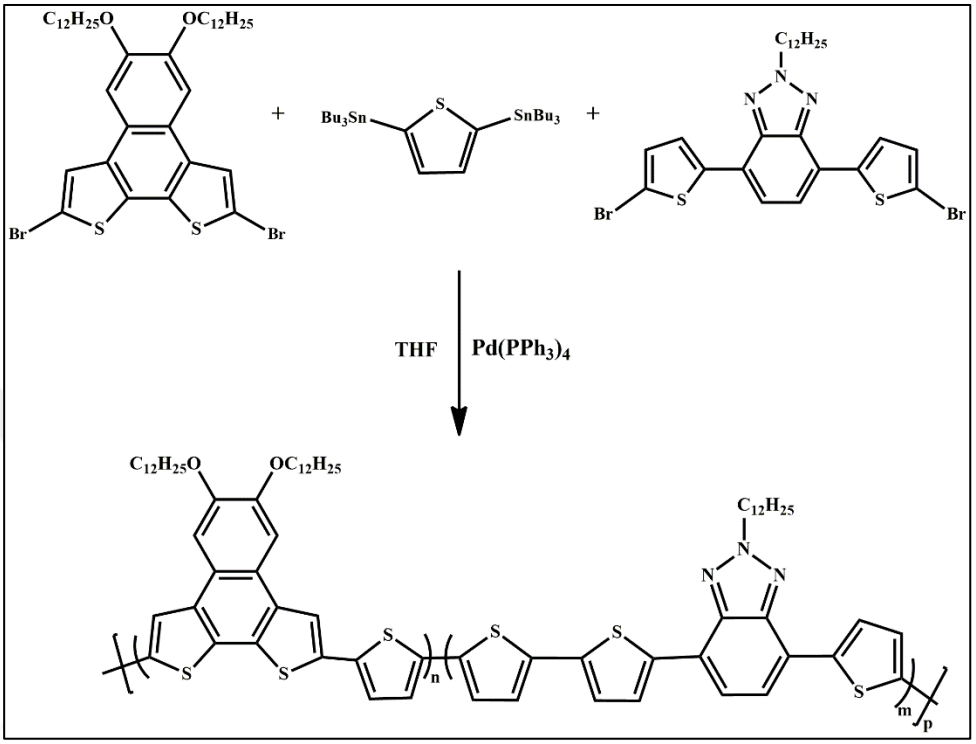

Figure 2.13. Synthetic route for P1

2,9-Dibromo-5,6-bis(dodecyloxy)naphtho[2,1-*b*:3,4-*b'*]dithiophene (100 mg, 0.13 mmol), 4,7-bis(5-bromothiophen-2-yl)-2-dodecyl-2H-benzo[*d*][1,2,3]triazole (79.5 mg, 0.13 mmol) and 2,5-bis(tributylstannyl)thiophene (173 mg, 0.26 mmol) were dissolved in anhydrous THF (15 mL) in a 50 mL two neck round bottom flask. To a stirred mixture $Pd(PPh_3)_4$ (5 mol %, 7.5 mg) was added and the solution was refluxed for 72 hours under argon atmosphere. The reaction was monitored with TLC and tributylstannyl thiophene (0.1 mL) was added as end-capper to remove bromine end groups and the reaction was stirred for overnight. Then bromobenzene (0.1 mL) was added to remove stannyl end groups and the reaction was stirred for another 6 hours. After completion of reaction, THF was evaporated under reduced pressure. The

resulting product was precipitated into methanol, filtrated and purified by Soxhlet extractor sequentially with methanol, acetone and hexane to remove oligomers and the residual catalyst. Polymer was extracted with chloroform, the solvent was concentrated and the polymer was precipitated from methanol. After filtration polymer was obtained as a red solid with 25 % yield.

M_n: 13 kDa, M_w: 16.5 kDa, PDI: 1.26

2.4.2. Synthesis of P2

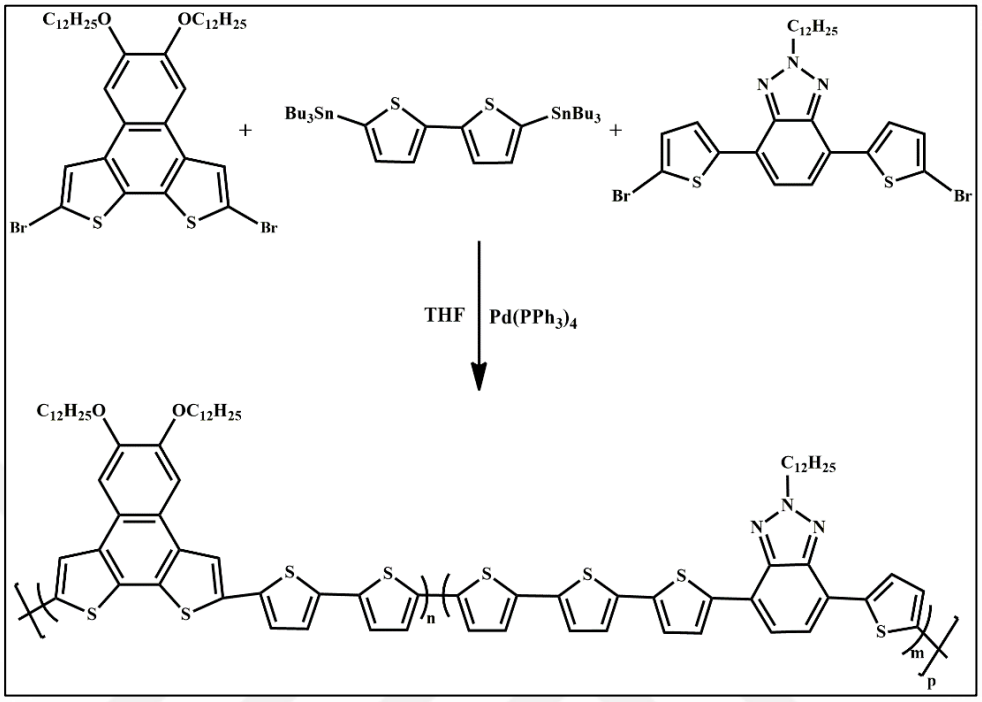

Figure 2.14. Synthetic route for P2

2,9-Dibromo-5,6-bis(dodecyloxy)naphtho[2,1-*b*:3,4-*b'*]dithiophene (118 mg, 0.15 mmol), 4,7-bis(5-bromothiophen-2-yl)-2-dodecyl-2H-benzo[*d*][1,2,3]triazole (93.8 mg, 0.13 mmol) and 5,5′-bis(tributylstannyl)-2,2′-bithiophene (227.8 mg, 0.31 mmol) were dissolved in anhydrous THF (15 mL) in a 50 mL two neck round bottom flask. To a stirred mixture $Pd(PPh_3)_4$ (5 mol %, 8.8 mg) was added and the solution was refluxed for 72 hours under argon atmosphere. The reaction was monitored with TLC and tributylstannyl thiophene (0.1 mL) was added as end-capper to remove bromine end groups and the reaction was stirred for overnight. Then bromobenzene (0.1 mL) was added to remove stannyl end groups and the reaction was stirred for another 6 hours. After completion of reaction, THF was evaporated under reduced pressure. The resulting product was precipitated into methanol, filtrated and purified by Soxhlet extractor sequentially with methanol, acetone and hexane to remove

oligomers and residual catalyst. Polymer was extracted with chloroform, the solvent was concentrated and the polymer was precipitated from methanol. After filtration polymer was obtained as dark red solid with 14 % yield.

^{1}H NMR (400 MHz, $CDCl_3$): δ 8.02, 7.82, 7.59, 7.51, 7.13, 7.04, 6.97, 6.73, 4.83, 4.23, 3.54, 2.35, 1.99, 1.25-1.43, 0.83

M_n: 12 kDa, M_w: 13.5 kDa, PDI: 1.10

2.5. Organic Solar Cell Device Fabrication

For organic solar cell application of polymers bulk-heterojunction type devices were constructed with ITO/PEDOT: PSS/Polymer: $PC_{70}BM$/LiF/Al device architecture. After ITO coated glass substrates were etched, cleaning process was applied to substrates to obtain smooth coating platform for PEDOT: PSS layer. Substrates were sonicated in ultrasonic bath with toluene, water-detergent mixture, water and isopropyl alcohol for 15 minutes each. After sonication, ITO substrates were dried via N_2 gun and oxygen plasma was applied to remove organic impurities. PEDOT: PSS was spin coated on the cleaned substrates as hole transport layer with 40 nm thickness. As the active layer, polymer and $PC_{70}BM$ solutions were prepared to form blends with different ratios in 1,2-dichlorobenzene. They were filtrated and spin coated onto PEDOT: PSS layer in a nitrogen gas filled glove-box system. After LiF (0.7 nm) and Al (~93 nm) were evaporated on active layer as cathode under 10^{-6} mbar pressure.

CHAPTER 3

RESULTS and DISCUSSION

3.1. Electrochemical Characterization of P1 and P2

In order to define redox behaviors of polymers and to determine HOMO and LUMO energy levels cyclic voltammetry (CV) studies were performed. Polymers were dissolved in chloroform and spray coated on ITO coated glass electrodes which function as the working electrode in a three-electrode cell system. Silver and platinum wires were employed as the reference and counter electrodes, respectively. Electrodes were dipped into a solution of 0.1 M Bu_4NPF_6/ACN electrolyte/solvent couple and CV studies of polymers were conducted at 100 mV/s scan rate.

Cyclic voltammetry studies revealed that P1 has only p-dopable character whereas P2 has both p-dopable and n-dopable natures. Through the potential scan of P1, oxidation potential was observed at 1.0 V followed by the reduction potential at 0.9 V. P2 demonstrated two reversible redox couples in p doping-dedoping processes. The first oxidation and reduction couple was observed at 0.9 V and 0.5 V while the second couple was observed at 1.3 V and 0.9 V. Lower oxidation potential of P2 than P1 was an expected result due to more electron rich nature of P2. Since P2 has also n-dopable character, n-type reversible redox couple was observed at -2.1 V and -1.7 V. Cyclic voltammograms of P1 and P2 are depicted in Figure 3.1. and Figure 3.2., respectively.

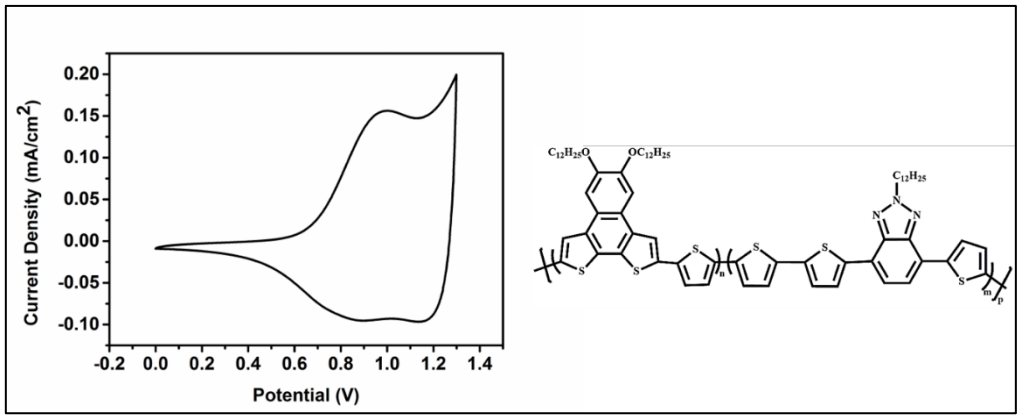

Figure 3.1. Cyclic voltammogram of P1 in 0.1 M Bu_4NPF_6 /ACN electrolyte/solvent couple at 100 mV/s scan rate

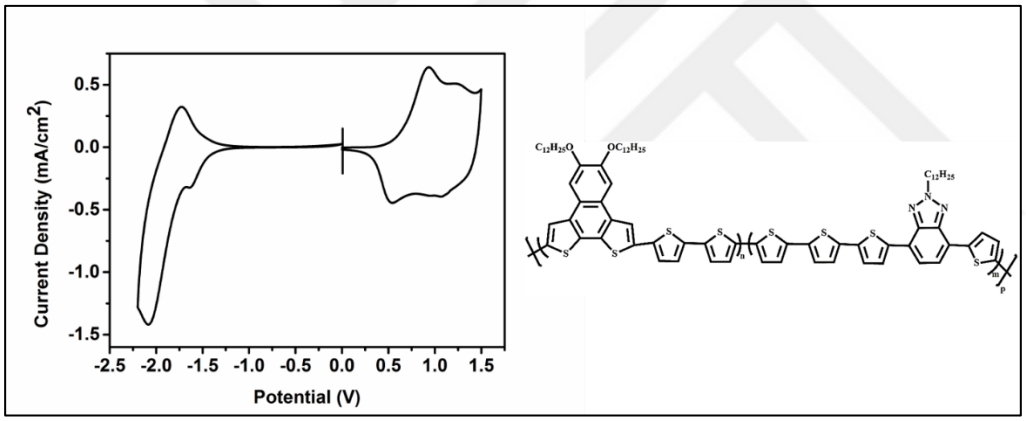

Figure 3.2. Cyclic voltammogram of P2 in 0.1 M Bu_4NPF_6 /ACN electrolyte/solvent couple at 100 mV/s scan rate

HOMO energy levels of both P1 and P2 were calculated from the onset of oxidation potentials which were determined from the intersection of baseline and tangent drawn to the oxidation peak. Onset of oxidation potential was placed in the equation below and corresponding HOMO levels of P1 and P2 were calculated as -5.4 eV and -5.3 eV.

$HOMO = -(4.75 + E^{ox}_{onset})$

HOMO levels of the polymers are close to each other since there is no great difference between their oxidation potentials. According to the results P1 has low-lying HOMO level compared to P2. Since P1 possesses only p-dopable character, LUMO energy level of -3.4 eV was calculated from the optical band gap and HOMO level. LUMO energy level of P2 however, was calculated from the onset of reduction potential due to its n-dopable nature. Reduction onset was placed in the similar equation and LUMO level was found as -3.1 eV. From the difference between HOMO and LUMO levels calculated from CV studies, electronic band gap of 2.2 eV was attained for P2. Results of electrochemical studies are summarized in Table 1.

Table 1. Summary of electrochemical properties of P1 and P2

	$E_{p\text{-doping}}$ (V)	$E_{p\text{-dedoping}}$ (V)	$E_{n\text{-doping}}$ (V)	$E_{n\text{-dedoping}}$ (V)	HOMO (eV)	LUMO (eV)	E_g^{el} (eV)
P1	1.0	0.9	-	-	-5.4	-3.4	-
P2	0.9/1.3	0.5/0.9	-2.1	-1.7	-5.3	-3.1	2.2

Cyclic voltammetry was also used to investigate the scan rate dependence of polymers. Scan rate studies reveal whether the anion compensation during doping-dedoping processes is diffusion controlled or not. Cyclic voltammograms were recorded with different scan rates in the same electrolyte and change in the current density was observed. It was not possible to perform scan rate study with P1 due to its low stability.

However linear relationship between scan rate and current density was observed for P2 proving that the anion compensation is non-diffusion controlled throughout doping-dedoping process. Scan rate dependence of P2 is demonstrated in Figure 3.3.

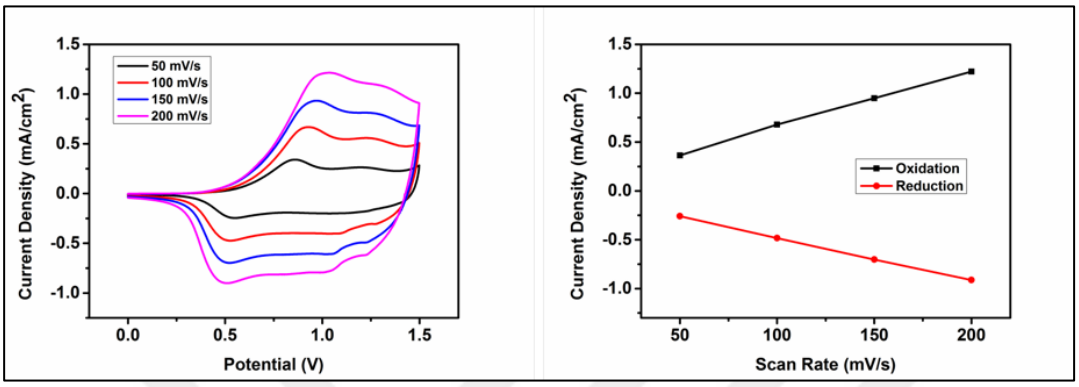

Figure 3.3. Scan rate dependence of P2

3.2. Spectroelectrochemical Characterization of P1 and P2

Spectroelectrochemical studies were performed to gain insight about changes in the electronic and optical properties of polymers upon doping process. Polymers dissolved in chloroform were spray coated onto ITO electrode and then polymer films were placed in 0.1 M Bu_4NPF_6/ACN electrolyte/solvent system. Changes in the absorption were monitored as a function of wavelength by increasing positive potential incrementally. Absorption maxima and optical wavelength were calculated from spectroelectrochemistry measurements.

For P1 potential was increased between 0 V and 1.3 V and for P2 gradual increase of potential was between 0 V and 1.2 V. The maximum absorption wavelengths were recorded at 470 nm for P1 and 450 nm for P2, respectively. These correspond to π-π* transitions of polymers. In order to calculate optical band gap of polymers from the equation of E_g^{op}= 1241/ λ_{onset}, the onsets of absorption maxima were determined as 606 nm and 613 nm for P1 and P2 respectively. Optical band gaps were calculated as

2.05 eV for P1 and 2.02 eV for P2. Even though, P1 has red-shifted absorption maxima it has slightly higher band gap than P2 due to lower λ_{onset}. It was expected that P2 could have red-shifted absorption maxima due to enhanced π-conjugation with incorporation of bithiophene unit in the polymer backbone rather than thiophene as in the case of P1. This unexpected situation may be aroused from the lower molecular weight of P2 in comparison with P1 causing decrease in the conjugation length. Still, higher λ_{onset} value of P2 leads to slight reduction in the optical band gap. Spectroelectrochemical characterization results are summarized in Table 2.

Table 2. Summary of spectroelectrochemical properties of P1 and P2

	λ_{max} **(nm)**	λ_{onset} **(nm)**	E_g^{op} **(eV)**
P1	470	606	2.05
P2	450	613	2.02

Gradual oxidation of polymer thin films with increasing potential caused the absorption in the visible region to decrease along with the formation of new absorption bands namely polarons and bipolarons in NIR region. These bands are the proof of formation of charge carriers during doping process. Intensity of polaronic and bipolaronic bands increases with the increase in applied potential. Formed polaron and bipolaron bands were around 720 nm and 1320 nm for P1 and 650 nm and 1060 nm for P2. UV-Vis-NIR spectra of polymers is demonstrated in Figure 3.4. and Figure 3.5.

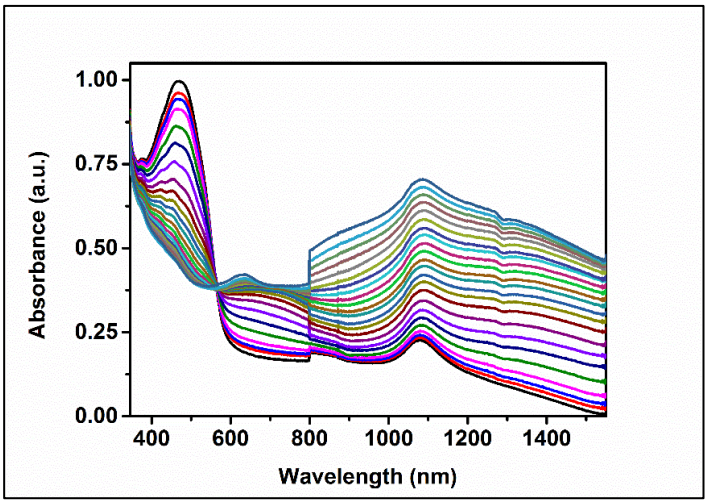

Figure 3.4. Electronic absorption spectra of P1 in 0.1 M Bu_4NPF_6/ACN solution between 0 V and 1.3 V

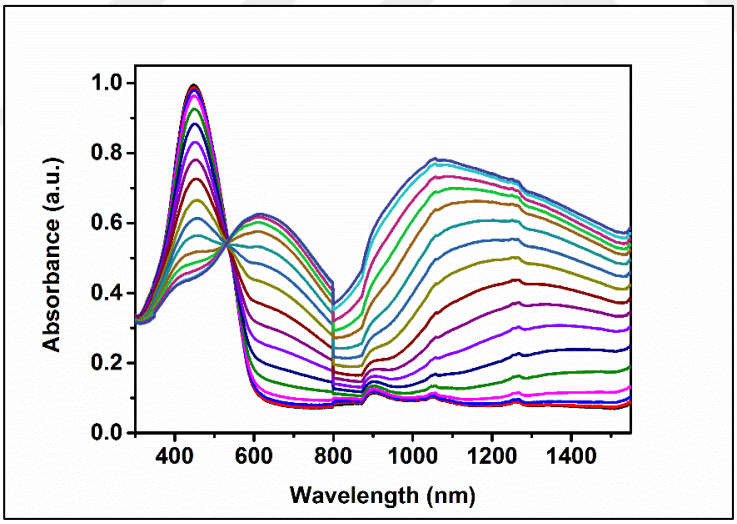

Figure 3.5. Electronic absorption spectra of P2 in 0.1 M Bu_4NPF_6/ACN solution between 0 V and 1.2 V

3.3. Colorimetric Characterization of P1 and P2

Polymers possess different colors in their neutral and doped states displaying electrochromic behavior. Formation of polarons and bipolarons with oxidation results in the color change of the polymers. In its neutral state P1 exhibits red-pink color whereas it has a transmissive grey color at its oxidized state. P2 displays an orange color in its neutral state, a blue color upon p-doping and a transmissive green/yellow color in n-doped state. In order to express colors in more accurate and scientific manner CIE (International Commission on Illumianation) coordinates were used with the parameters of L, a, b. Here L corresponds to luminance, a corresponds to red/green color and b corresponds to yellow/blue color. Colors of the polymer thin films is demonstrated in Figure 3.6. and L,a,b values are reported at Table 3.

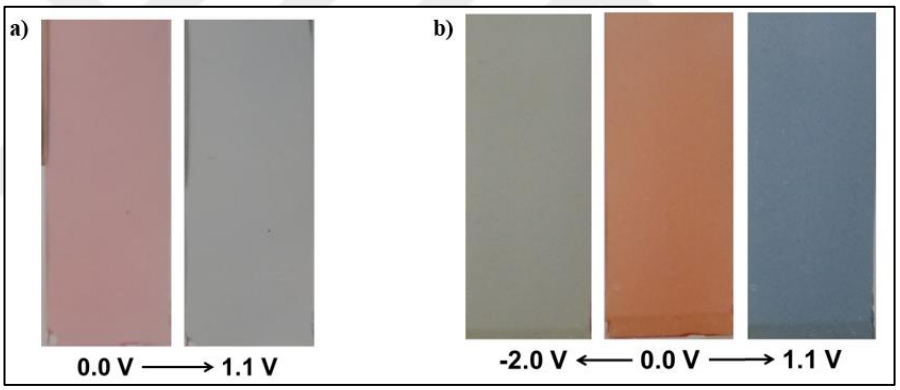

Figure 3.6. Colors of a) P1 and b) P2 at different potentials.

Table 3. L,a,b measurements of P1 and P2

	Applied Potential	L	a	b
P1	**0.0 V**	60	14	6
	1.1 V	61	0	1
P2	**0.0 V**	56	22	25
	1.1 V	49	-4	-12
	-2.0 V	58	-1	5

3.4. Optical properties of P1 and P2

Optical properties of polymers were investigated in solid state as thin film and in chloroform solution. In thin film form absorption maxima was obtained at 470 nm and 450 nm for P1 and P2 as mentioned before. In chloroform solution however maximum absorption of 435 nm for P1 and 445 nm for P2 was observed (Table 4).

Table 4. Summary of optical properties of P1 and P2

	λ_{max}(thin film) (nm)	λ_{max}(solution) (nm)
P1	470	435
P2	450	445

Both polymers demonstrated red shift in the absorption maxima from solution to the thin film form which is much more pronounced in the case of P1 showing 35 nm red shift. In contrast to P1, P2 showed unremarkable red shift in the order of 5 nm however P2 showed broadened absorption in solid state. The reason for the red shift displayed in solid state is due to the better aggregation of molecules in solid form and enhanced π-π stacking in solid state. Small red shift in case of P2 may result from the similarity of molecular aggregation in solution and in solid state. Enhanced π-π stacking in solution demonstrated by P2 may result from lowered steric hindrance. In P1 alkyl chains in NDT and benzotriazole units are in close proximity which may create steric hindrance preventing π-π stacking in solution and therefore a considerable red shift was observed in solid state. However, in P2 π bridge of bithiophene unit eliminates steric hindrance. Absorption spectra of polymers in solution and in thin film is displayed in Figure 3.7.

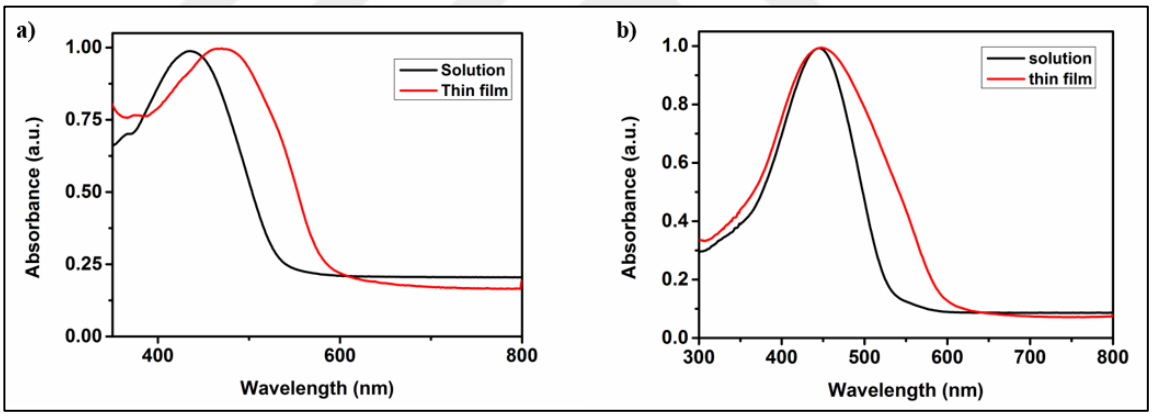

Figure 3.7. UV-Vis spectra of a) P1 and b) P2 in chloroform solution and in thin film

3.5. Kinetic Properties of P1 and P2

In order to determine optical contrast and switching time of the corresponding polymers kinetic studies were conducted. Optical contrast in electrochromic materials

is generally reported as the percent transmittance change. Kinetic studies were performed with polymer coated ITO electrodes in a solution of 0.1 M Bu_4NPF_6/ACN and the change in percent transmittance was recorded by applying neutral and fully oxidized state potentials to the polymers with 5 second time intervals at specified wavelengths which were previously determined from UV-Vis-NIR spectra. For P1 only percent transmittance change of 11 % at 1320 nm was observed due to stability issues of polymer in the visible region during kinetic studies. Percent transmittance changes of 34 % at 450 nm, 43 % at 650 nm and 57 % at 1060 nm were obtained for P2 with fair stabilities. Switching time is the time necessary for electrochromic material to change its color between neutral and oxidized states at 95 % contrast to which human eye is sensitive. Calculated switching time for P1 was 1.0 s at 1320 nm. For P2 1.6 s at 450 nm, 0.9 s at 650 nm and 0.7 s at 1060 nm were attained. Switching time in NIR region is faster for P2 than P1. Optical contrast and switching time values are summarized in Table 5 and depicted in Figure 3.8 and Figure 3.9. From P1 to P2 improvements in both optical contrast and switching time were achieved. Stability problems of P1 in kinetic studies may be aroused from the steric hindrance due to long alkyl chains in the polymer backbone which are in close proximity when thiophene is incorporated as π- bridge. However, replacing bithiophene with thiophene as a π-bridge could lower steric hindrance and doping-dedoping process becomes more facile leading enhanced kinetic properties for P2.

Table 5. Summary of optical contrast and switching times of P1 and P2

	Optical contrast (ΔT %)		**Switching times (s)**
P1	11	1320 nm	1.0
P2	34	450 nm	1.6
	43	650 nm	0.9
	57	1060 nm	0.7

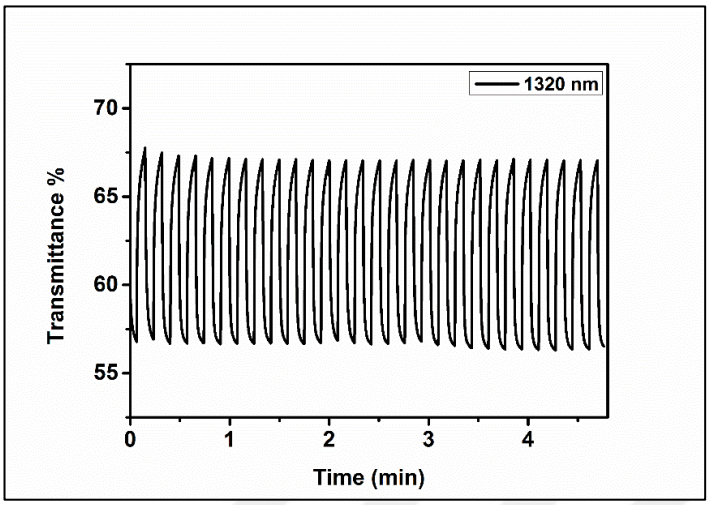

Figure 3.8. Percent transmittance change of P1 in 0.1 M Bu_4NPF_6/ACN solution at maximum absorption wavelength

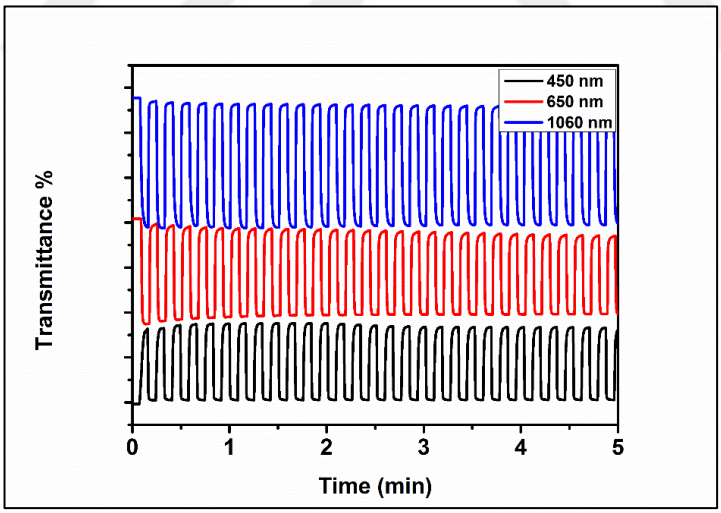

Figure 3.9. Percent transmittance change of P2 in 0.1 M Bu_4NPF_6/ACN solution at maximum absorption wavelengths

3.6. Organic Solar Cell Applications

Both P1 and P2 were synthesized to be used as active layers in organic photovoltaic devices. Organic solar cell devices were constructed from both of the polymers however P1 did not show any efficiency due to its poor film formation. Additionally, low absorption coefficient of P1 might prevent absorption of necessary number of photons to generate photocurrent.

Organic solar device architecture of ITO/PEDOT:PSS/P2:$PC_{71}BM$/LiF/Al was pursued in the construction. Relative energy level of solar cell device for P2 is given in Figure 3.10. As acceptor in constructed bulk-heterojunction solar cell devices, $PC_{71}BM$ was the choice due to its light absorption capability in visible region [85]. Studies were carried out in terms of optimizing weight ratio of P2 and $PC_{71}BM$ blend by preparing solutions in o-DCB with different ratios. Results are summarized in Table 6 and J-V curve recorded for different P2: $PC_{71}BM$ ratios is given in Figure 3.11. Best power conversion efficiency of 1.17 % was obtained with 1:1 ratio of P2: $PC_{71}BM$ blend. It is clear from the results that with the decrease in $PC_{71}BM$ ratio in the blend short-circuit current increases. Since J_{sc} is highly influenced from effective photon absorption, with more contribution of polymer in the blend light harvesting of active layer enhances in case of P2 resulting improved J_{sc}. Highest FF of 41 % was found for best operating device may indicate improved active layer morphology for 1:1 blend ratio.

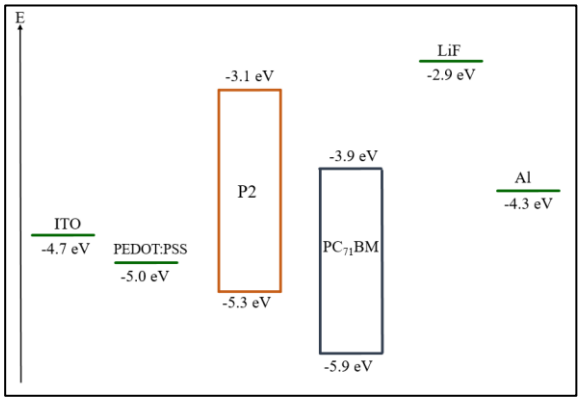

Figure 3.10. Energy level diagram of ITO/PEDOT: PSS/P2: $PC_{71}BM$/LiF/Al device

Table 6. Summary of organic solar cell studies

P2: $PC_{71}BM$	V_{oc} (V)	Jsc (mA/cm^2)	V_{mp} (V)	I_{mp} (mA/cm^2)	FF (%)	PCE (%)
1:1	0.59	4.85	0.32	3.68	41	1.17
1:2	0.56	4.17	0.36	2.43	37	0.87
1:3	0.55	3.78	0.36	2.27	39	0.81

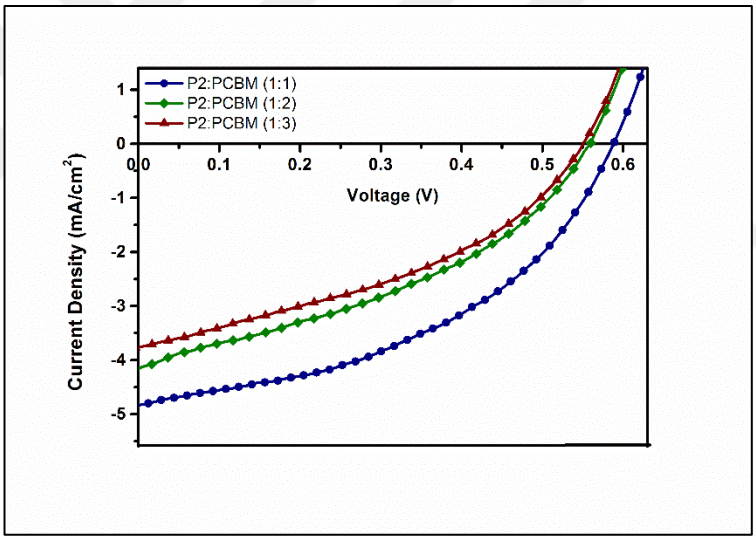

Figure 3.11. J-V curve of P2

Molecular weight of donor is known to have influence on photovoltaic properties of the operating device. Higher molecular weights provide effective conjugation through the polymer backbone leading reduced band gaps which facilitates absorption of more solar light [86]. Low molecular weight of P2 and consequently moderate band gap can be reasons of reduced PCE compare to those of NDT based polymers in the literature. Therefore, with the increase in molecular weight enhanced efficiency can be obtained

from NDT and benzotriazole based random copolymers. However, from P1 to P2 enhanced electron delocalization in terms of change in π-bridge created much better performance for the organic solar cell device. Steric hindrance in the polymer backbone of P1 could cause charge carriers to be trapped and no generation of photocurrent from the solar cell device.

Incident photon to current efficiency measurement was performed to understand the relation between the collected charge carrier amount and incident photon amount. IPCE is described as the ratio of these two parameters. Measurement was performed with the best operating device between 350 nm and 1000 nm with monochromatic light calibrated against silicon photodiode. For the photovoltaic device with 1:1 ratio of P2: $PC_{71}BM$ blend maximum IPCE was found as 17.88 % demonstrated in Figure 3.12.

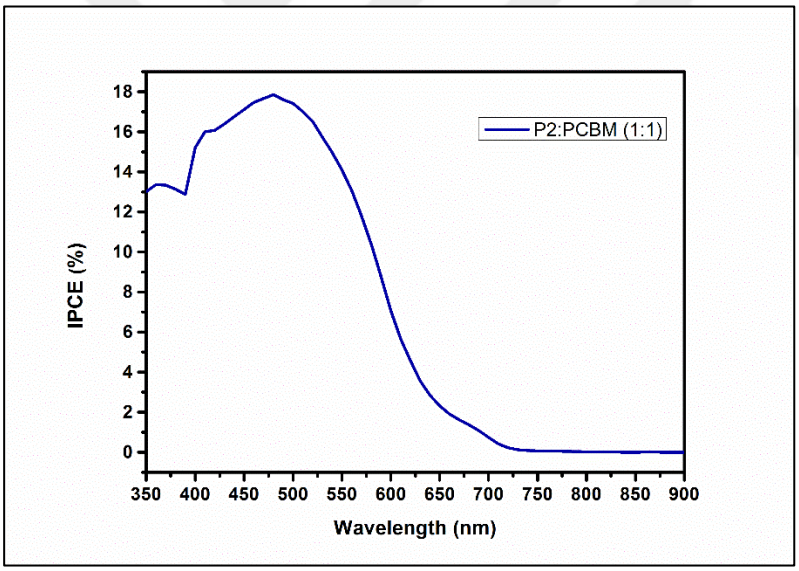

Figure 3.12. IPCE curve for 1:1 P2: $PC_{71}BM$ device

CHAPTER 4

CONCLUSION

Two novel donor-acceptor type random copolymers bearing naphtho[2,3-*b*:3,4-*b'*]dithiophene and benzotriazole units were designed and synthesized via Stille cross-coupling reaction. In order to investigate change in optoelectronic properties, two different π-bridges were incorporated into polymer backbone namely thiophene and bithiophene. Electrochemical, spectroelectrochemical and optical characterizations of random copolymers were successfully completed and the polymers were used as light harvesting layer in organic solar cell applications.

Electrochemical characterization studies revealed that P1 has only p-dopable character whilst P2 possesses ambipolar character. HOMO energy levels were calculated as -5.4 eV and -5.3 eV for P1 and P2. LUMO energy level of P1 was estimated from optical band gap due to its p-dopable nature and for P2 it was calculated from CV due to ambipolar character. Calculated LUMO levels were -3.4 eV and -3.1 eV for P1 and P2. Optical band gaps and absorption maxima of polymers were determined from spectroelectrochemistry studies. Formation of polaron and bipolaron regions with the decrease in neutral absorption through incrementally increased potential was also monitored with spectroelectrochemical studies. Optical band gaps were calculated as 2.05 eV and 2.02 eV for P1 and P2. Since P2 has lower molecular weight red shift in the visible absorption was observed with P1 instead of P2. Colorimetric studies were conducted and colors of the polymers in neutral and doped states were proved by L,a,b values. Optical contrast and switching time studies were performed. From P1 to P2 considerable improvements in percent transmittance and switching time was observed. For P1 percent transmittance of 11 % and switching time of 1.0 s were calculated only in NIR region due to its instability. For P2 at 450 nm 34 %, at 650 nm 43% and at 1060

nm 57% optical contrasts were calculated with 1.6 s, 0.9 s and 0.7 s switching times, respectively. Reason for this improved results in P2 were attributed to the elimination of steric hindrance problem resulting from thiophene bridge which was replaced with bithiophene bridge in P2.

Bulk-heterojunction solar cell was constructed with both P1 and P2 however no photocurrent was generated when P1 was used as active layer. This might be resulted from close proximity of alkyl chains in the polymer backbone creating steric hindrance and therefore causing ineffective charge separation and charge transport. However, bithiophene incorporated P2 demonstrated 1.17 % maximum power conversion efficiency when used as active layer. The result is promising for NDT and benzotriazole bearing random copolymer since P2 has low molecular weight where effective conjugation length is decreased. However, it is possible to enhance PCE with increasing molecular weight via optimizations in synthesis. After all, from P1 to P2 both electrochemical, spectroelectrochemical and photovoltaic properties were improved and it can be deduced that change of π-bridge from thiophene to bithiophene has positive effect on polymer structure and properties.

REFERENCES

[1] F. Carpi, D. De Rossi, Opt. Laser Technol. 38 (2006) 292–305.

[2] T.M. Clarke, J.R. Durrant, Chem. Rev. 110 (2010) 6736–6767.

[3] S.R. Forrest, M.E. Thompson, Chem. Rev. 107 (2007) 1985–1987.

[4] C.K. Chiang, C.R. Fincher, Y.W. Park, A.J. Heeger, H. Shirakawa, E.J. Louis, S.C. Gau, A.G. MacDiarmid, Phys. Rev. Lett. 39 (1977) 1098–1101.

[5] H. Shirakawa, Angew. Chem. Int. Ed. Volume 40 (2001) 2574–2580.

[6] A.J. Heeger, 125 (2000) 380–417.

[7] A.G. MacDiarmid, Angew. Chemie Int. Ed. 40 (2001) 2581–2590.

[8] H. Jiang, P. Taranekar, J.R. Reynolds, K.S. Schanze, Angew. Chemie Int. Ed. 48 (2009) 4300–4316.

[9] G. Yu, J. Gao, J.C. Hummelen, F. Wudl, A.J. Heeger, Science 270 (1995) 1789–1791.

[10] G. Horowitz, Adv. Mater. 10 (1998) 365–377.

[11] J.H. Burroughes, D.D.. Bradley, A.R. Brown, R.N. Marks, K. Mackay, R.H. Friend, P.L. Burns, A.B. Holmes, Nature 347 (1990) 539–541.

[12] L. Dou, J. You, Z. Hong, Z. Xu, G. Li, R.A. Street, Y. Yang, Adv. Mater. 25 (2013) 6642–6671.

[13] H.A.M. van Mullekom, J.A.J.M. Vekemans, E.E. Havinga, E.W. Meijer, Mat. Sci. Eng. R. 32 (2001) 1–40.

[14] L. Dou, Y. Liu, Z. Hong, G. Li, Y. Yang, Chem. Rev. 115 (2015) 12633–12665.

[15] J. Roncali, Macromol. Rapid Commun. 28 (2007) 1761–1775.

[16] B.C. Thompson, Y.G. Kim, T.D. McCarley, J.R. Reynolds, J. Am. Chem. Soc.

128 (2006) 12714–12725.

[17] K. Colladet, S. Fourier, T.J. Cleij, L. Lutsen, J. Gelan, D. Vanderzande, L. HuongNguyen, H. Neugebauer, S. Sariciftci, a Aguirre, G. Janssen, E. Goovaerts, Macromolecules 40 (2007) 65–72.

[18] Y.-J. Cheng, S.-H. Yang, C.-S. Hsu, Chem. Rev. 109 (2009) 5868–5923.

[19] R.J. Mortimer, Chem. Soc. Rev. Chem. Soc. Rev 26 (1997) 147–156.

[20] A.A. Argun, P.H. Aubert, B.C. Thompson, I. Schwendeman, C.L. Gaupp, J. Hwang, N.J. Pinto, D.B. Tanner, A.G. MacDiarmid, J.R. Reynolds, Chem. Mater. 16 (2004) 4401–4412.

[21] R.J. Mortimer, Electrochim. Acta 44 (1999) 2971–2981.

[22] S.K. Deb, Appl. Opt. 8 (1969) 192–195.

[23] P.R. Somani, S. Radhakrishnan, Mater. Chem. Phys. 77 (2012) 117–133.

[24] C.L. Bird, A.T. Kuhn, Chem. Soc. Rev. 10 (1981) 49–82.

[25] R.J. Mortimer, A.L. Dyer, J.R. Reynolds, Displays 27 (2006) 2–18.

[26] S. Sapp, G. Sotzing, J.R. Reynolds, Chem. Mater. 10 (1998) 2101–2108.

[27] P.M. Beaujuge, J.R. Reynolds, Chem. Rev. 110 (2010) 268–320.

[28] K.C. Nicolaou, P.G. Bulger, D. Sarlah, Angew. Chemie - Int. Ed. 44 (2005) 4442–4489.

[29] J.L. Reddinger, J.R. Reynolds, Radic. Polym. Polyelectrolytes 145 (1999) 57–122.

[30] B. Carsten, F. He, H.J. Son, T. Xu, L. Yu, Chem. Rev. 111 (2011) 1493–1528.

[31] Z. Bao, W.K. Chan, L. Yu, J. Am. Chem. Soc. 117 (1995) 12426–12435.

[32] C. Li, Z. Bo, in:, F.; Huang, H.-L. Yip;, Y. Cao (Eds.), Polym. Photovoltaics Mater. Physics, Device Eng., Royal Society of Chemistry, 2015, pp. 1–31.

[33] R. Martin, S.L. Buchwald, Acc. Chem. Res. 41 (2008) 1461–1473.

[34] A.A.C. Braga, N.H. Morgon, G. Ujaque, F. Maseras, J. Am. Chem. Soc. 127 (2005) 9298–9307.

[35] J. Sakamoto, M. Rehahn, G. Wegner, A.D. Schlüter, Macromol. Rapid Commun. 30 (2009) 653–687.

[36] A. Suzuki, J. Organomet. Chem. 653 (2002) 83–90.

[37] D. Wöhrle, D. Meissner, Adv. Mater. 3 (1991) 129–138.

[38] E. Bundgaard, F.C. Krebs, Sol. Energy Mater. Sol. Cells 91 (2007) 954–985.

[39] J.-M. Nunzi, Comptes Rendus Phys. 3 (2002) 523–542.

[40] H. Spanggaard, F.C. Krebs, Sol. Energy Mater. Sol. Cells 83 (2004) 125–146.

[41] N. Yeh, P. Yeh, Renew. Sustain. Energy Rev. 21 (2013) 421–431.

[42] R. Kroon, M. Lenes, J.C. Hummelen, P.W.M. Blom, B. de Boer, Polym. Rev. 48 (2008) 531–582.

[43] H. Hoppe, N.S. Sariciftci, J. Mater. Res. 19 (2004) 1924–1945.

[44] C.W. Tang, Appl. Phys. Lett. 48 (1986) 183–185.

[45] S. Gunes, H. Neugebauer, N.S. Sariciftci, Chem. Rev. 107 (2007) 1324–1338.

[46] P. Kumar, S. Chand, Prog. Photovolt Res. Appl. 20 (2012) 377–415.

[47] C. Winder, N.S. Sariciftci, J. Mater. Chem. 14 (2004) 1077–1086.

[48] M.C. Scharber, N.S. Sariciftci, Prog. Polym. Sci. 38 (2013) 1929–1940.

[49] H. Hoppe, M. Niggemann, C. Winder, J. Kraut, R. Hiesgen, A. Hinsch, D. Meissner, N.S. Sariciftci, Adv. Funct. Mater. 14 (2004) 1005–1011.

[50] A.C. Mayer, S.R. Scully, B.E. Hardin, M.W. Rowell, M.D. McGehee, Mater. Today 10 (2007) 28–33.

[51] R. Jean, Acc. Chem. Res. 42 (2009) 1719–1730.

[52] T.L. Benanti, D. Venkataraman, Photosynth. Res. 87 (2006) 73–81.

[53] B. Qi, J. Wang, J. Mater. Chem. 22 (2012) 24315–24325.

[54] M.C. Scharber, D. Mühlbacher, M. Koppe, P. Denk, C. Waldauf, A.J. Heeger, C.J. Brabec, Adv. Mater. 18 (2006) 789–794.

[55] R.S. Kularatne, H.D. Magurudeniya, P. Sista, M.C. Biewer, M.C. Stefan, J. Polym. Sci. Part A Polym. Chem. 51 (2013) 743–768.

[56] D. Gupta, S. Mukhopadhyay, K.S. Narayan, Sol. Energy Mater. Sol. Cells 94 (2010) 1309–1313.

[57] B. Qi, J. Wang, Phys.Chem.Chem.Phys. 15 (2013) 8972–8982.

[58] H. Zhou, L. Yang, W. You, Macromolecules 45 (2012) 607–632.

[59] T.-Y. Chu, J. Lu, S. Beaupre, Y. Zhang, J.-R. Pouliot, S. Wakim, J. Zhou, M. Leclerc, Z. Li, J. Ding, Y. Tao, J. Am. Chem. Soc. 133 (2011) 4250–4253.

[60] M. Zhang, Y. Gu, X. Guo, F. Liu, S. Zhang, L. Huo, T.P. Russell, J. Hou, Adv. Mater. 25 (2013) 4944–4949.

[61] J. You, L. Dou, K. Yoshimura, T. Kato, K. Ohya, T. Moriarty, K. Emery, C.-C. Chen, J. Gao, G. Li, Y. Yang, Nat. Commun. 4 (2013) 1446.

[62] J. Yuan, J. Gu, G. Shi, J. Sun, H.-Q. Wang, W. Ma, Sci. Rep. 6 (2016) 26459.

[63] H. Zhou, Y. Zhang, C.K. Mai, S.D. Collins, G.C. Bazan, T.Q. Nguyen, A.J. Heeger, Adv. Mater. 27 (2015) 1767–1773.

[64] J.-S. Wu, S.-W. Cheng, Y.-J. Cheng, C.-S. Hsu, Chem. Soc. Rev. 44 (2015) 1113–1154.

[65] Z. Wu, T. Yang, B.S. Ong, Y. Liang, X. Guo, Org. Photonics Photovoltaics 2 (2014) 21–39.

[66] X. Zhu, K. Lu, H. Li, R. Zhou, Z. Wei, Chinese Chem. Lett. (2016).

[67] S. Loser, C.J. Bruns, H. Miyauchi, R.P. Ortiz, A. Facchetti, S.I. Stupp, T.J.

Marks, J. Am. Chem. Soc. 133 (2011) 8142–8145.

[68] Q. Peng, Q. Huang, X. Hou, P. Chang, J. Xu, S. Deng, Chem. Commun. 48 (2012) 11452–11454.

[69] S.R. Sanjaykumar, S. Badgujar, C.E. Song, W.S. Shin, S. Moon, I. Kang, J. Lee, S. Cho, S.K. Lee, J. Lee, Macromolecules 45 (2012) 6938–6945.

[70] R.S. Koti, S.R. Sanjaykumar, S. Hong, C. Eun, I. Kang, S. Kyu, W. Suk, S. Moon, J. Lee, Sol. Energy Mater. Sol. Cells 108 (2013) 213–222.

[71] P. Dutta, W. Yang, S.H. Eom, W.-H. Lee, I.N. Kang, S.-H. Lee, Chem. Commun. 48 (2012) 573–575.

[72] I. Osaka, T. Abe, M. Shimawaki, T. Koganezawa, K. Takimiya, ACS Macro Lett. 1 (2012) 437–440.

[73] P. Dutta, H. Park, W.-H. Lee, I.N. Kang, S.-H. Lee, Polym. Chem. 5 (2014) 132–143.

[74] S. Shi, P. Jiang, S. Yu, L. Wang, X. Wang, M. Wang, H. Wang, Y. Li, X. Li, J. Mater. Chem. A. 1 (2013) 1540–1543.

[75] X. Li, G. Yu, Y. Li, Macromolecules 46 (2013) 3358–3366.

[76] C. Bathula, C.E. Song, S. Badgujar, S.-J. Hong, S.Y. Park, W.S. Shin, J.-C. Lee, S. Cho, T. Ahn, S.-J. Moon, S.K. Lee, Polym. Chem. 4 (2013) 2132–2139.

[77] I. Osaka, T. Kakara, N. Takemura, T. Koganezawa, K. Takimiya, J. Am. Chem. Soc. 135 (2013) 8834–8837.

[78] S.W. Cheng, C.E. Tsai, W.W. Liang, Y.L. Chen, F.Y. Cao, C.S. Hsu, Y.J. Cheng, Macromolecules 48 (2015) 2030–2038.

[79] S.Q. Xiao, H.X. Zhou, W. You, Macromolecules 41 (2008) 5688–5696.

[80] N. Kleinhenz, L. Yang, H. Zhou, S.C. Price, W. You, Macromolecules 44 (2011) 872–877.

[81] B. Wang, S.-W. Tsang, W. Zhang, Y. Tao, M.S. Wong, Chem. Commun. (Camb). 47 (2011) 9471–9473.

[82] Y.J. Kim, Y.-J. Lee, J.-W. Jang, H. Cha, Y.-H. Kim, S.-K. Kwon, C.E. Park, J. Polym. Sci. Part A Polym. Chem. 51 (2013) 4742–4751.

[83] A. Balan, D. Baran, G. Gunbas, A. Durmus, F. Ozyurt, L. Toppare, Chem. Commun. (Camb). 60 (2009) 6768–6770.

[84] Y. Xia, Y. Li, Y. Zhu, J. Li, P. Zhang, J. Tong, C. Yang, H. Li, D. Fan, J. Mater. Chem. C 2 (2014) 1601–1604.

[85] M.M. Wienk, J.M. Kroon, W.J.H. Verhees, J. Knol, J.C. Hummelen, P.A. van Hal, R.A.J. Janssen, Angew. Chem. Int. Ed. Engl. 42 (2003) 3371–3375.

[86] K. Vandewal, S. Himmelberger, A. Salleo, Macromolecules 46 (2013) 6379–6387.

APPENDIX A

NMR SPECTRA

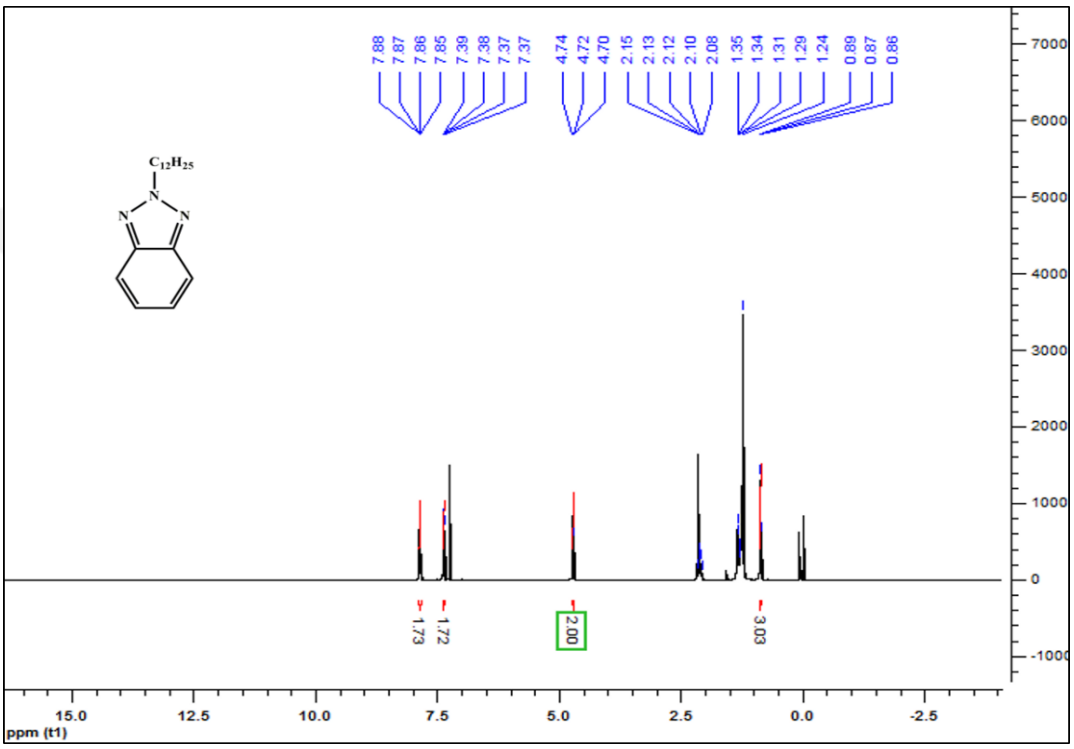

Figure A.1. ^{1}H-NMR spectrum of 2-dodecyl-2H-benzo[*d*][1,2,3]triazole

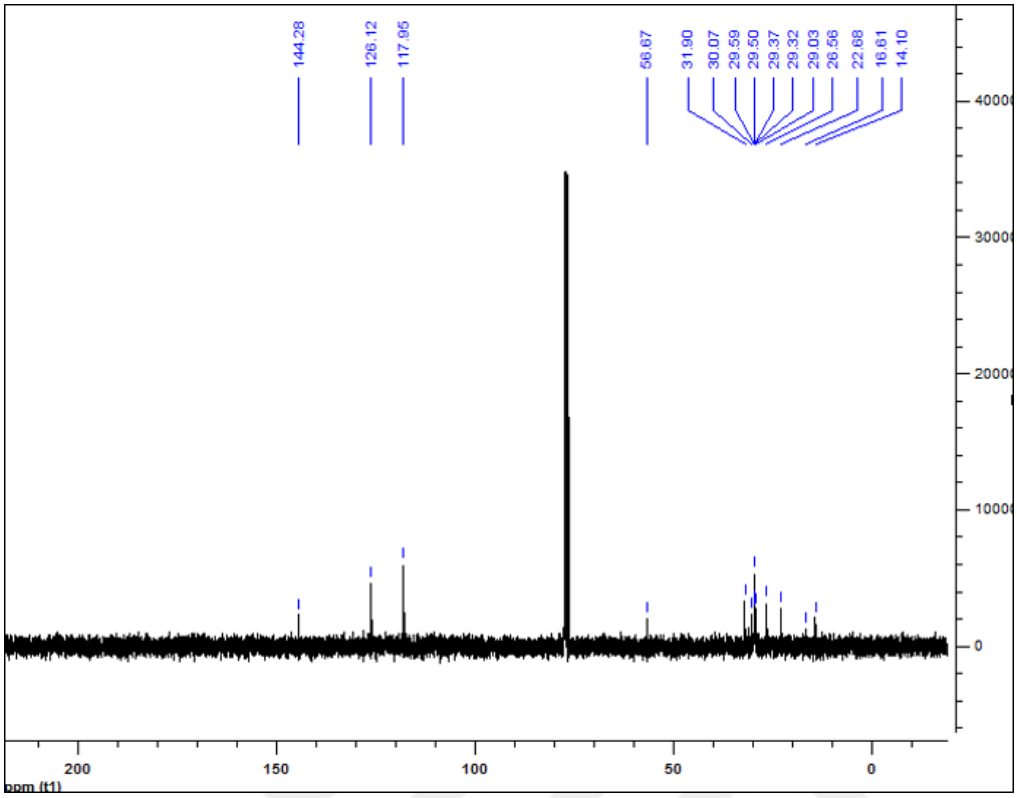

Figure A.2. ^{13}C -NMR spectrum of 2-dodecyl-2H-benzo[*d*][1,2,3]triazole

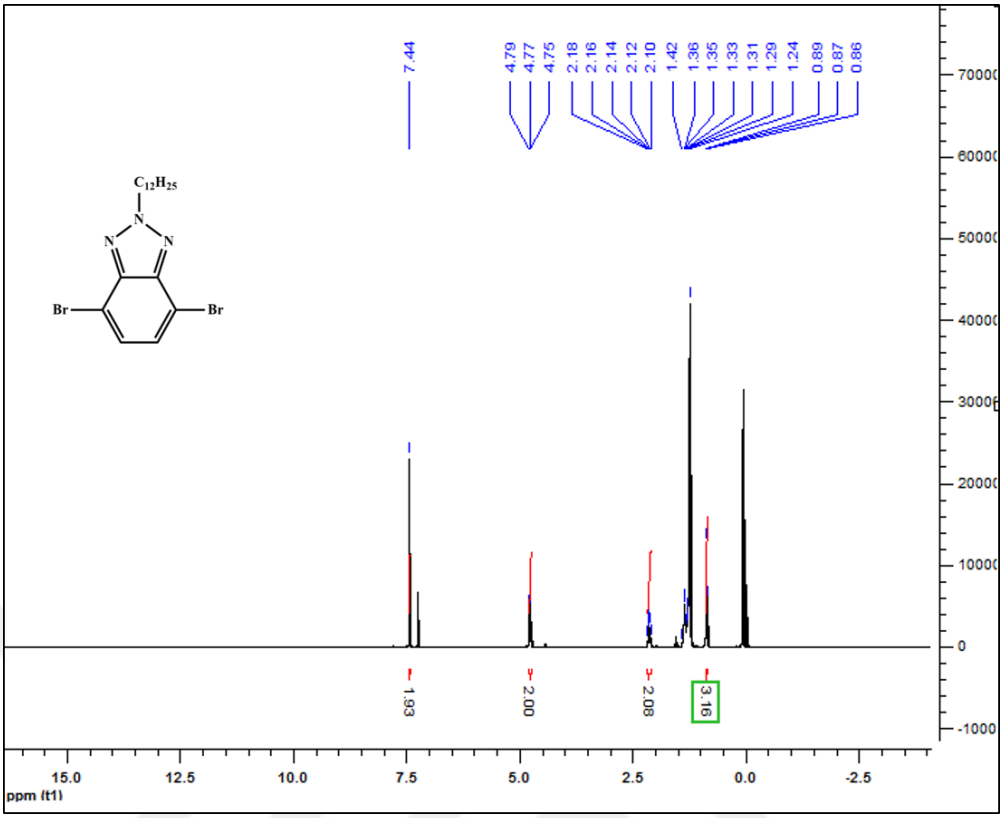

Figure A.3. ^{1}H-NMR spectrum of 4,7-dibromo-2-dodecyl-2H-benzo[*d*][1,2,3]triazole

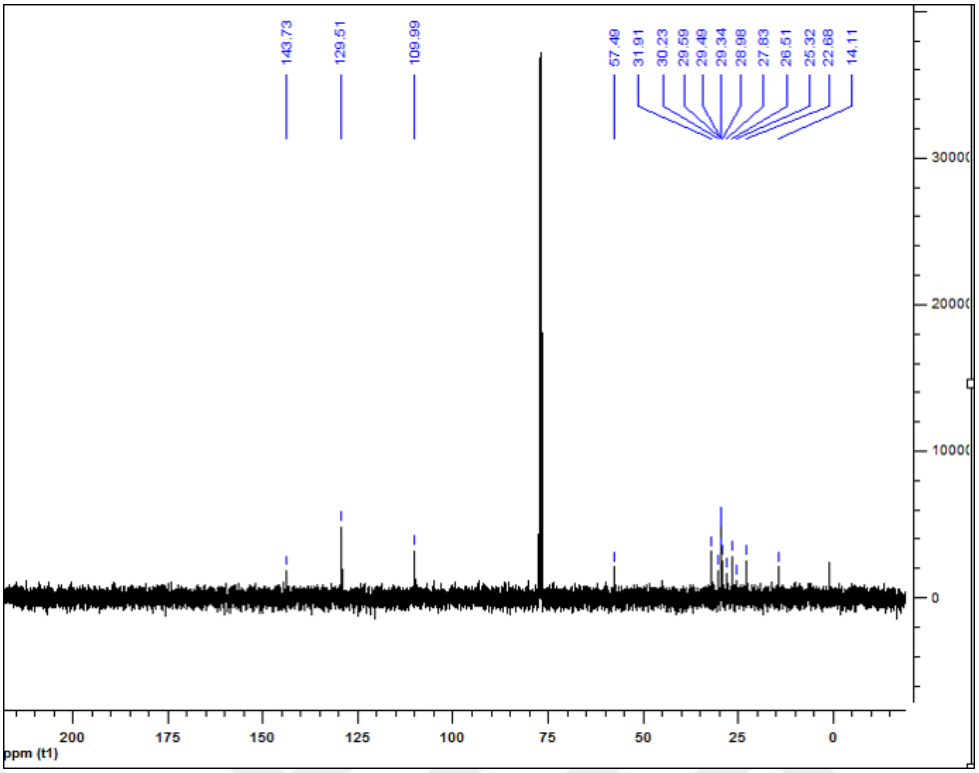

Figure A.4. ^{13}C-NMR spectrum of 4,7-dibromo-2-dodecyl-2H-benzo[*d*][1,2,3]triazole

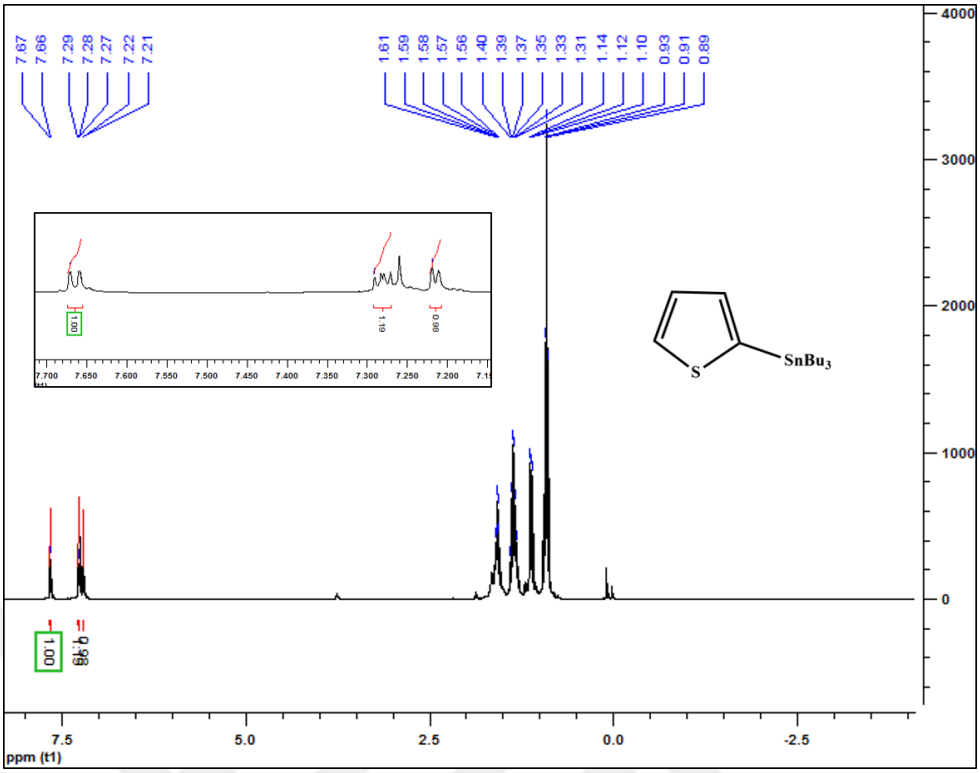

Figure A.5. ^{1}H-NMR spectrum of tributyl(thiophen-2-yl)stannane

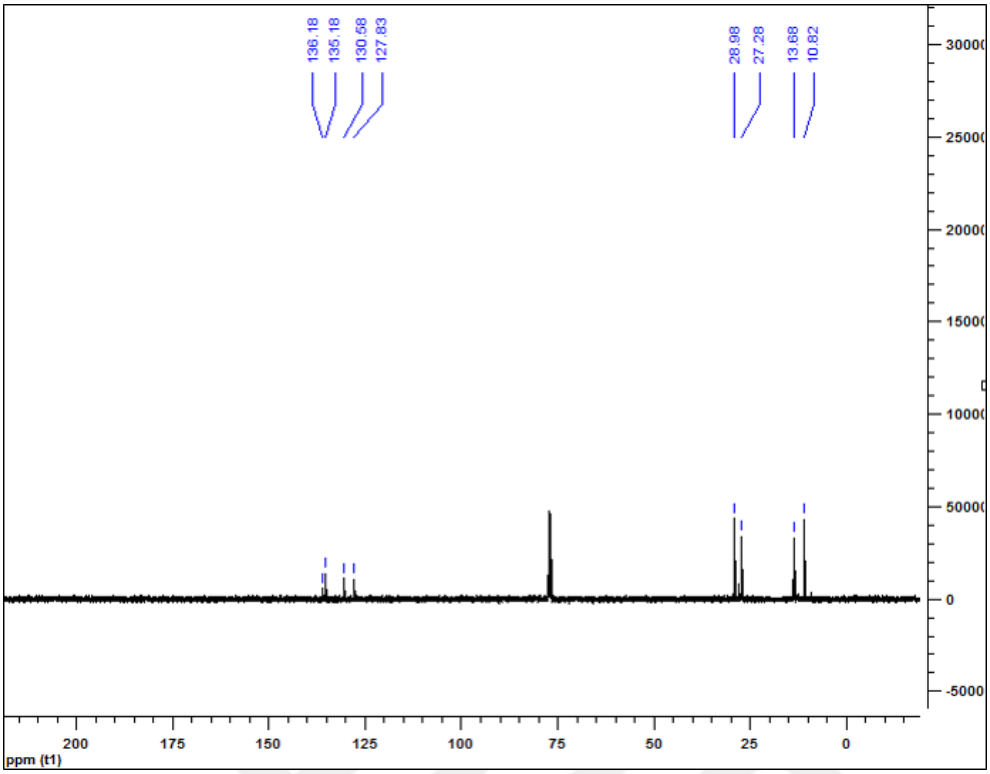

Figure A.6. ^{13}C-NMR spectrum of tributyl(thiophen-2-yl)stannane

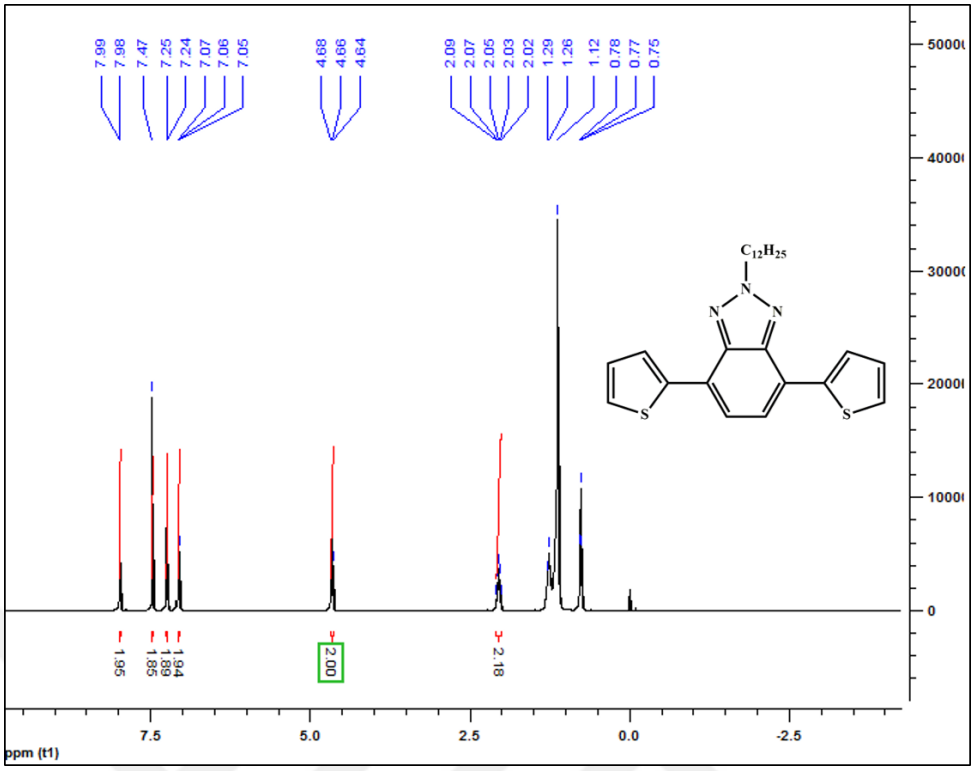

Figure A.7. ^{1}H-NMR spectrum of 2-dodecyl-4,7-di(thiophen-2-yl)-2H-benzo[*d*][1,2,3]triazole

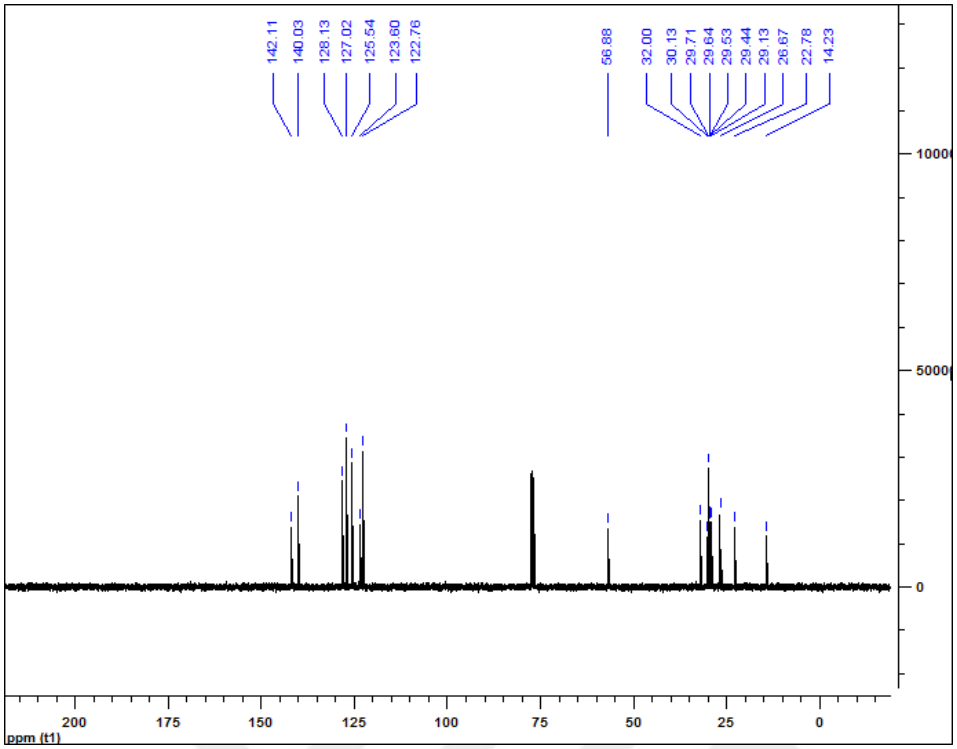

Figure A.8. ^{13}C-NMR spectrum of 2-dodecyl-4,7-di(thiophen-2-yl)-2H-benzo[*d*][1,2,3]triazole

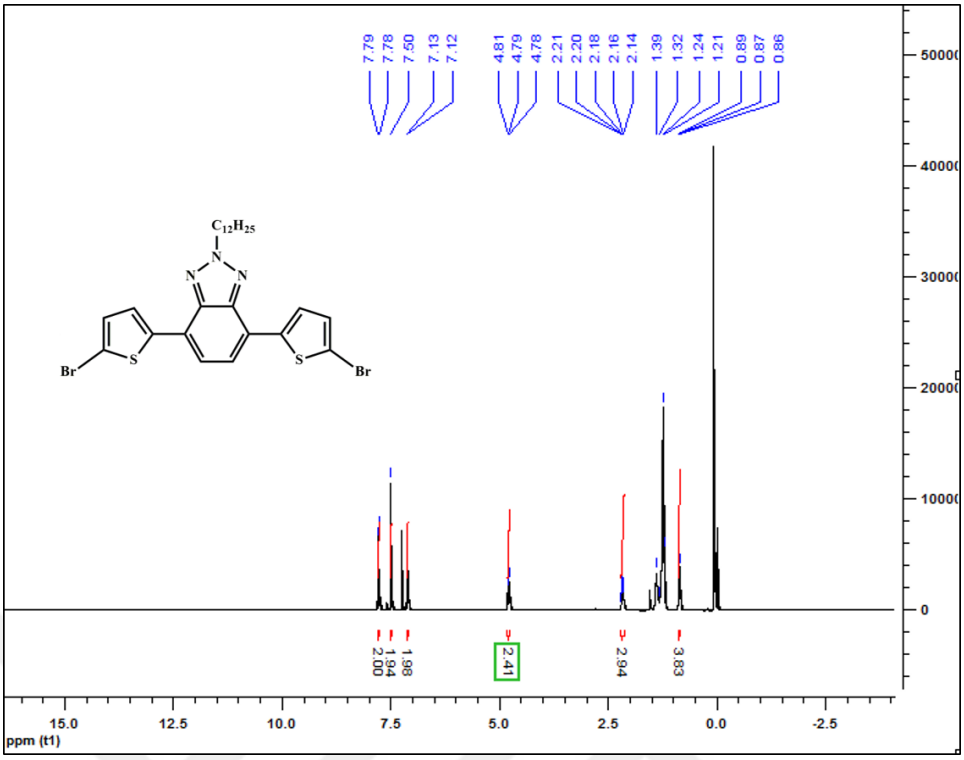

Figure A.9. ^{1}H-NMR spectrum of 4,7-bis(5-bromothiophen-2-yl)-2-dodecyl-2H-benzo[*d*][1,2,3]triazole

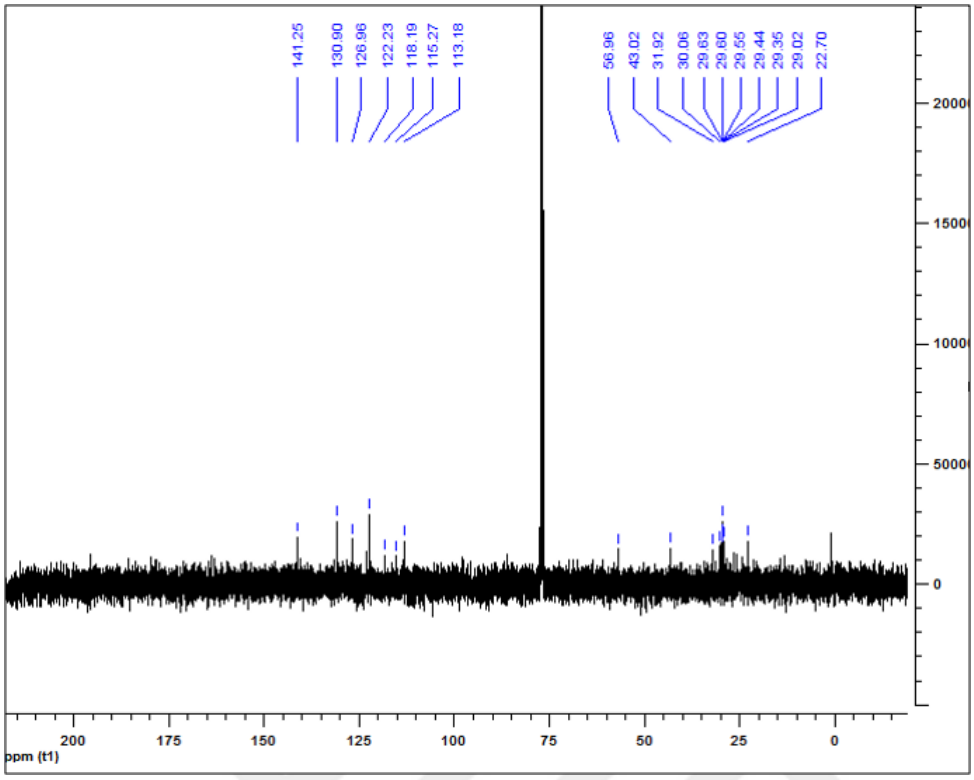

Figure A.10. ^{13}C-NMR spectrum of 4,7-bis(5-bromothiophen-2-yl)-2-dodecyl-2H-benzo[*d*][1,2,3]triazole

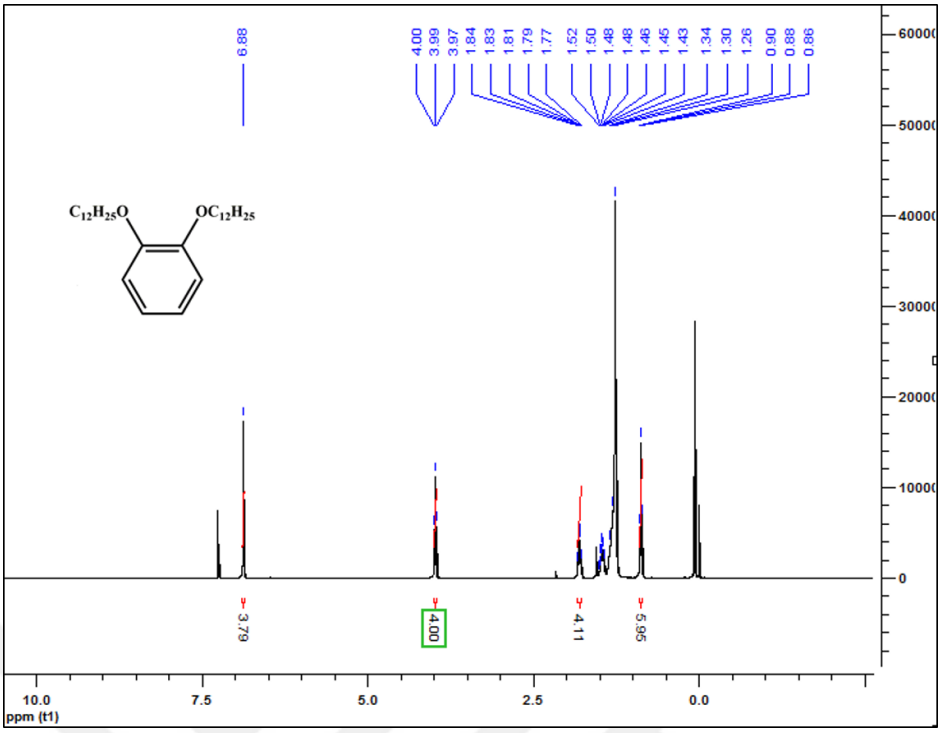

Figure A.11. ^{1}H-NMR spectrum of 1,2-bis(dodecyloxy)benzene

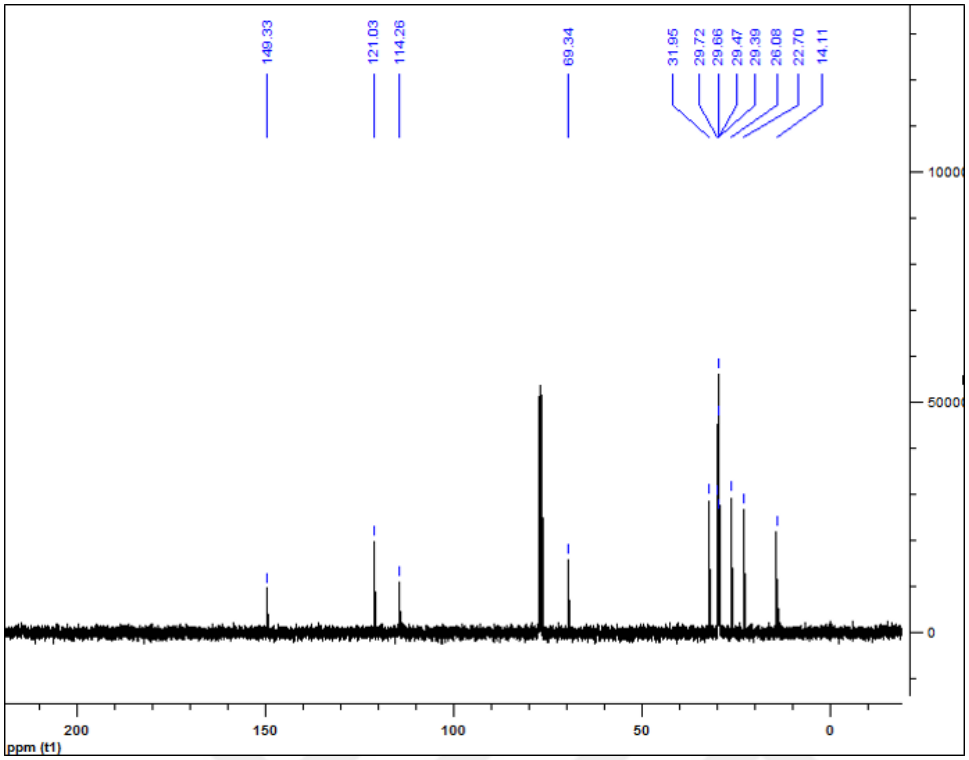

Figure A.12. ^{13}C-NMR spectrum of 1,2-bis(dodecyloxy)benzene

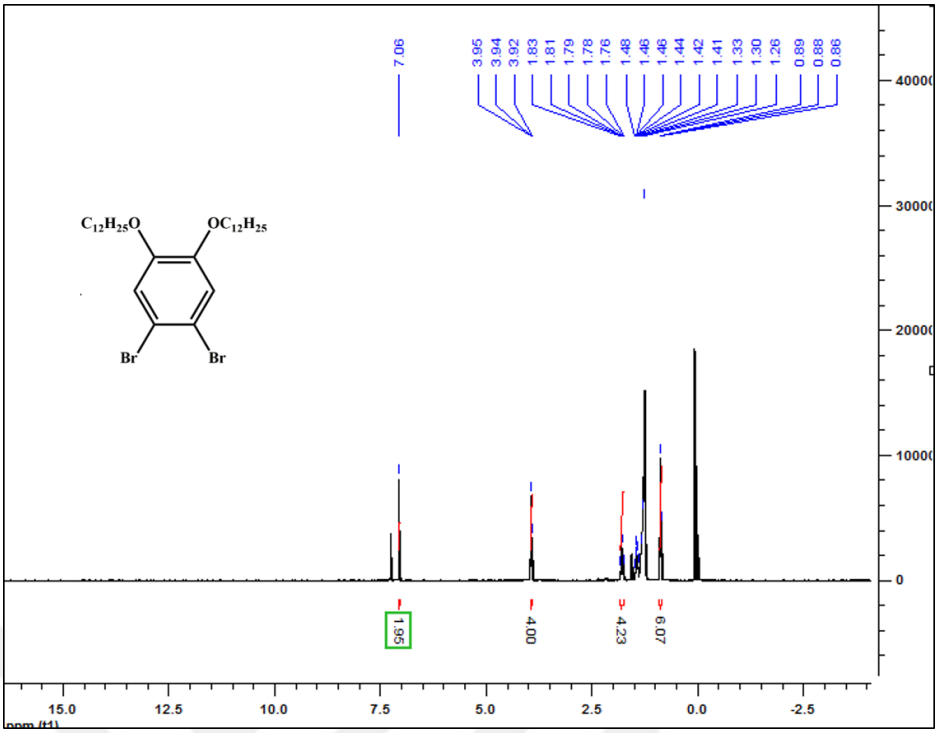

Figure A.13. ^{1}H-NMR spectrum of 1,2-dibromo-4,5-bis(dodecyloxy)benzene

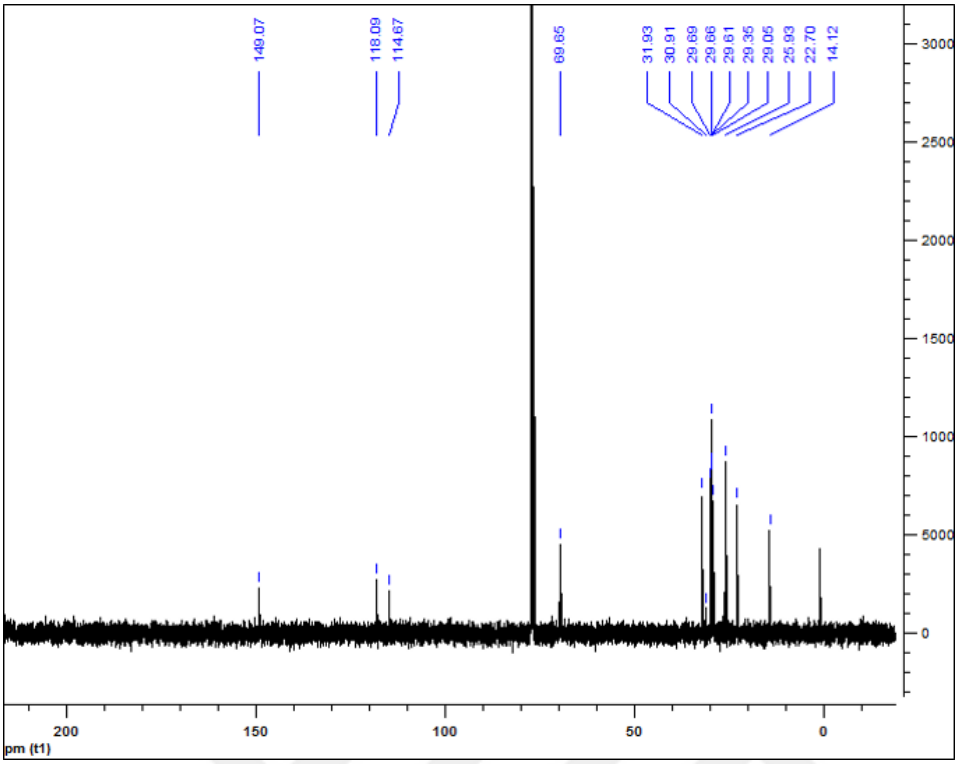

Figure A.14. ^{13}C-NMR spectrum of 1,2-dibromo-4,5-bis(dodecyloxy)benzene

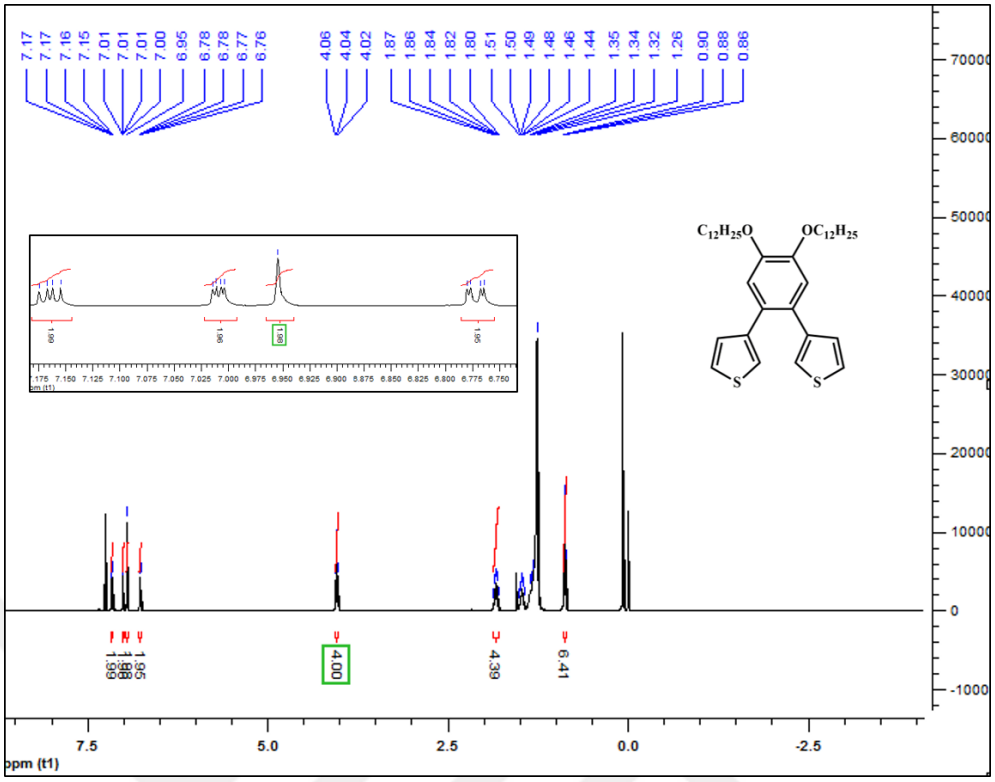

Figure A.15. ^{1}H-NMR spectrum of 3,3'-(4,5-bis(dodecyloxy)-1,2-phenylene)dithiophene

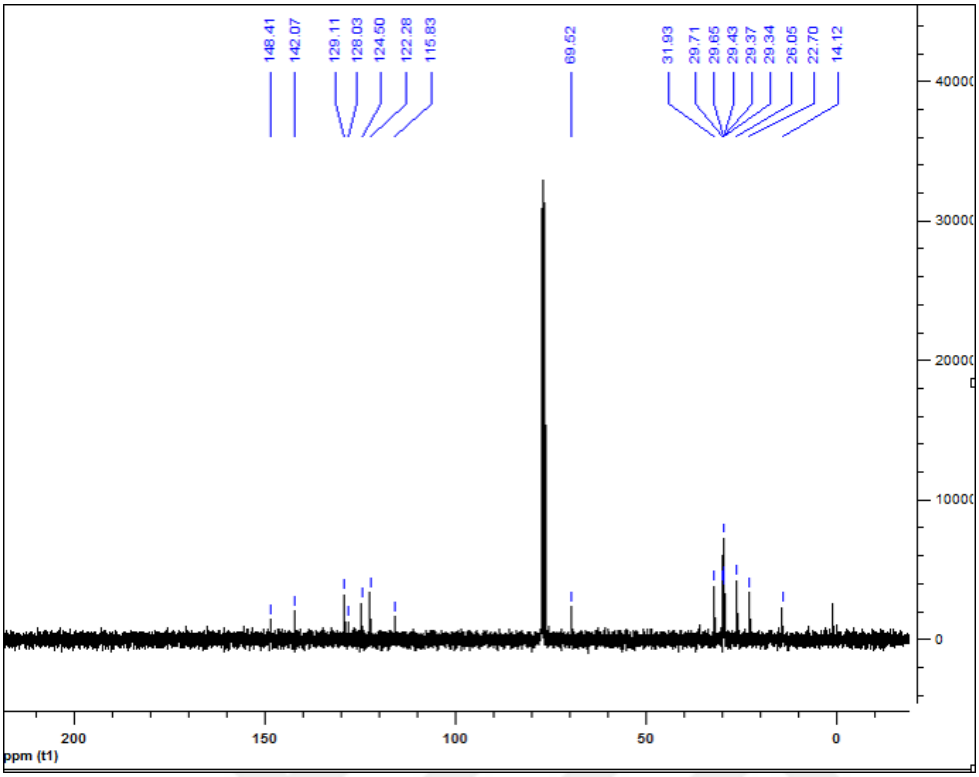

Figure A.16. ^{13}C-NMR spectrum of 3,3'-(4,5-bis(dodecyloxy)-1,2-phenylene)dithiophene

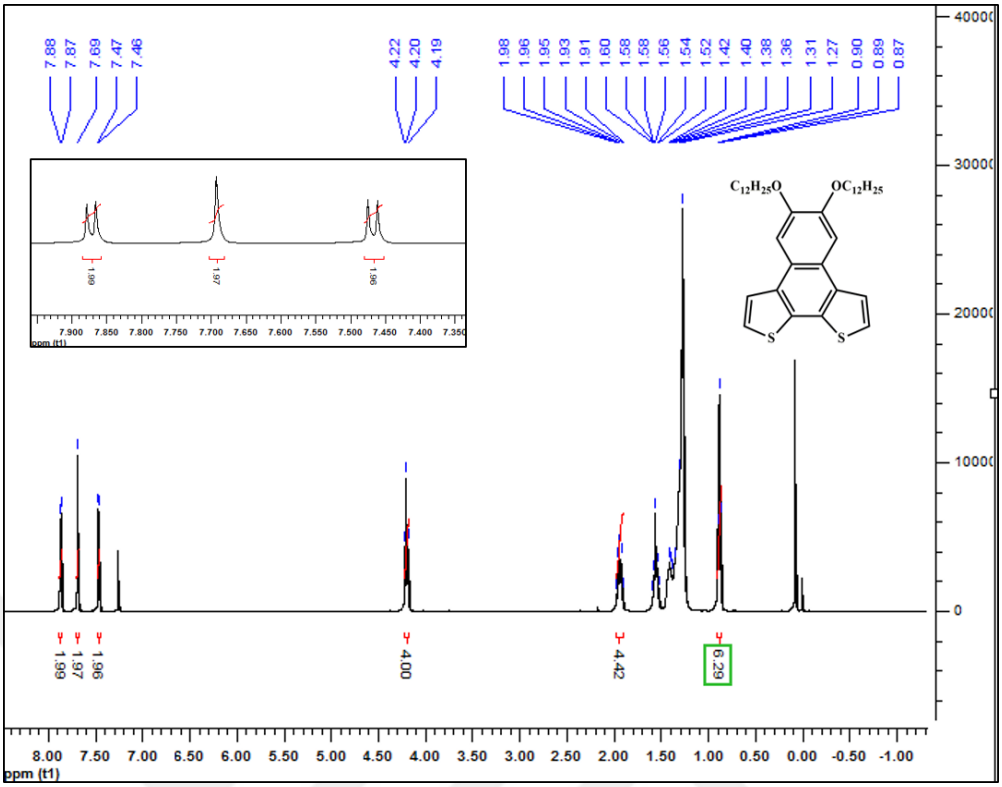

Figure A.17. ^{1}H-NMR spectrum of 5,6-bis(dodecyloxy)naphtho[2,1-*b*:3,4-*b'*]dithiophene

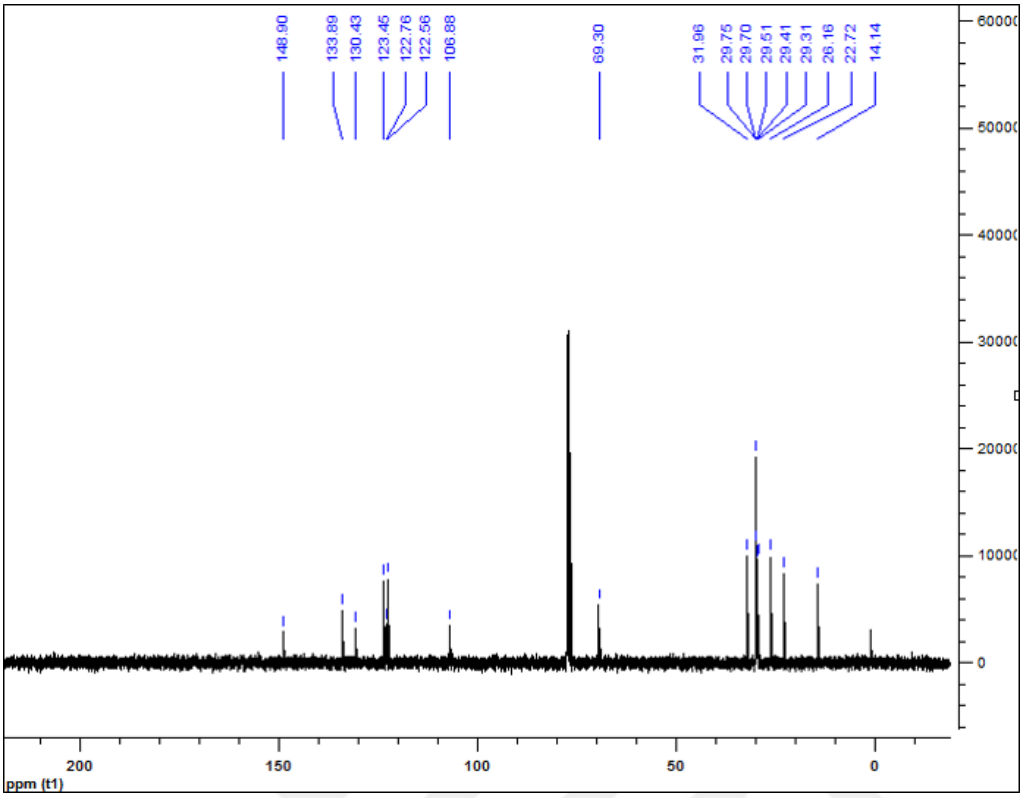

Figure A.18. ^{13}C-NMR spectrum of 5,6-bis(dodecyloxy)naphtho[2,1-*b*:3,4-*b'*]dithiophene

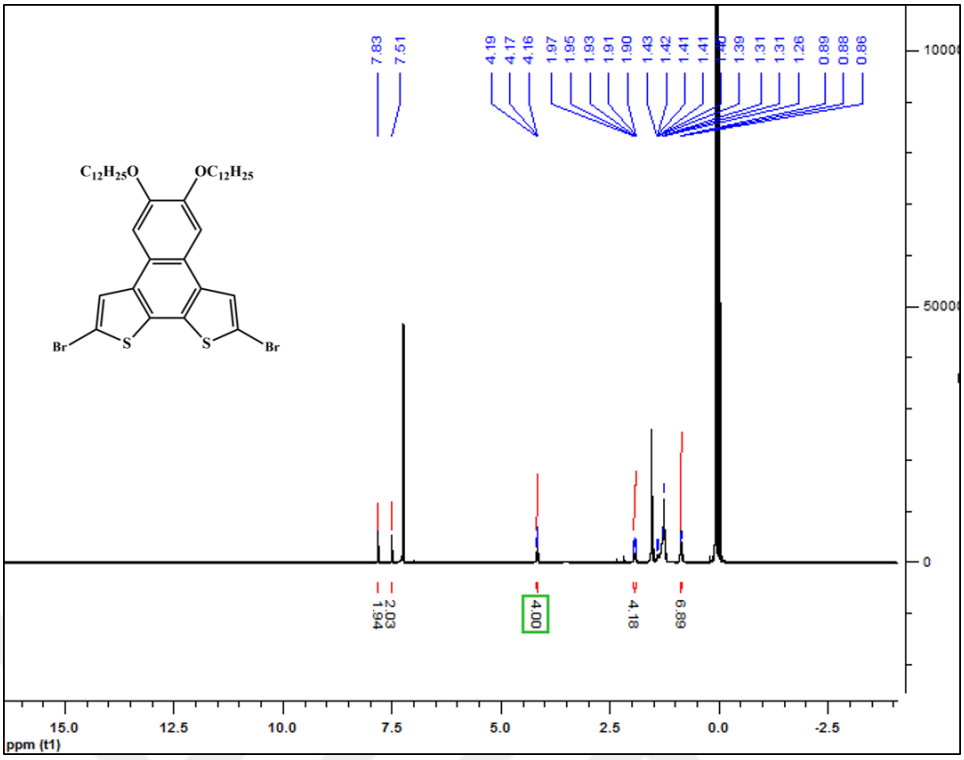

Figure A.19. ^{1}H-NMR spectrum of 2,9-dibromo-5,6-bis(dodecyloxy)naphtho[2,1-*b*:3,4-*b*']dithiophene

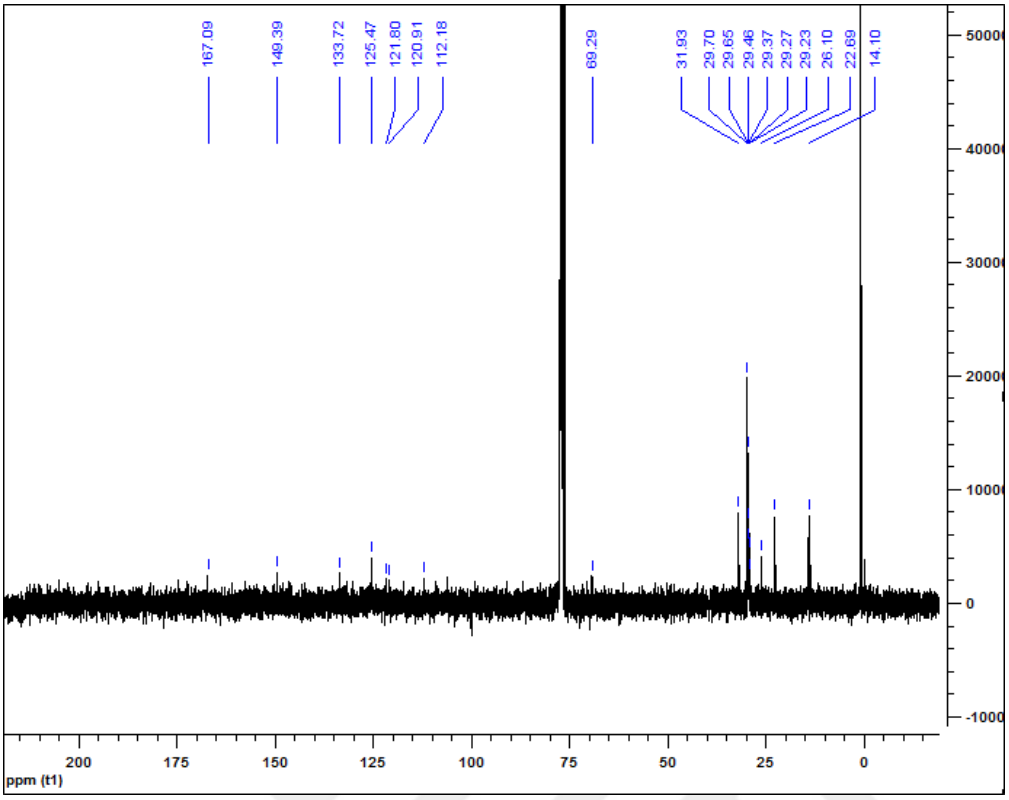

Figure A.20. ^{13}C-NMR spectrum of 2,9-dibromo-5,6-bis(dodecyloxy)naphtho[2,1-*b*:3,4-*b'*]dithiophene

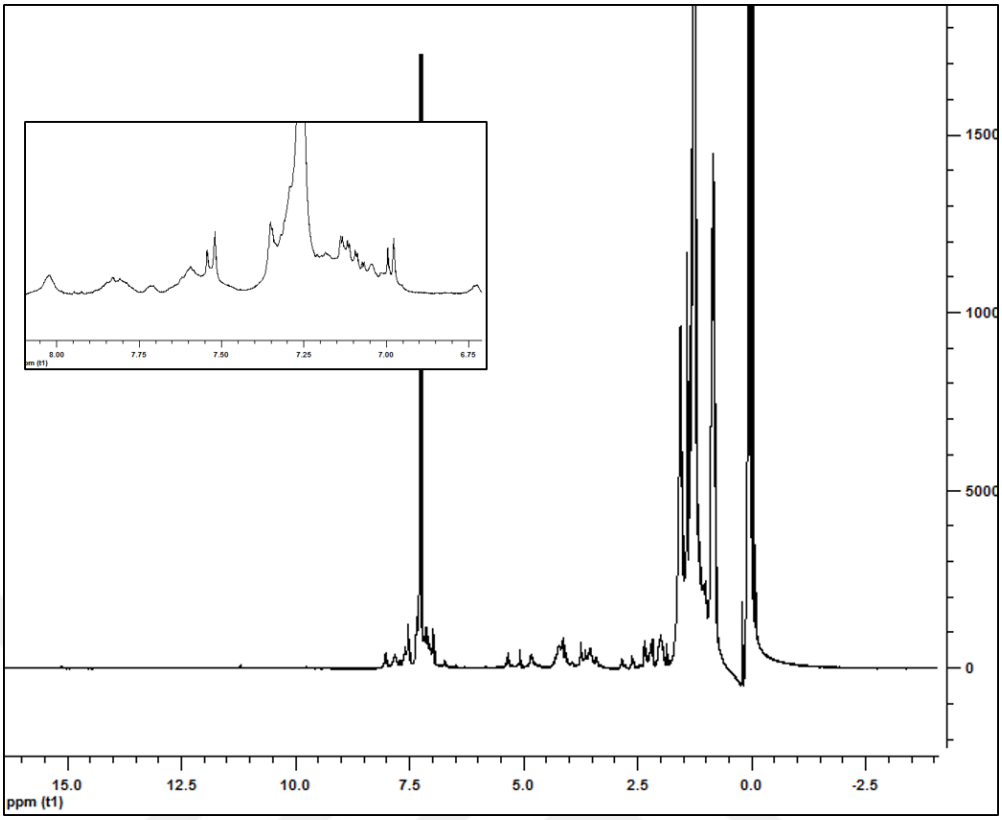

Figure A.21. ^{1}H-NMR spectrum of P2